UNIVERSITY OF CALIFORNIA, SAN DIEGO

Order And Disorder In Spin Systems

A dissertation submitted in partial satisfaction of the
requirements for the degree
Doctor of Philosophy

in

Physics

by

Yury Kiselev

Committee in charge:

Professor Daniel P. Arovas, Chair
Professor Eric E. Fullerton
Professor John A. McGreevy
Professor David A. Meyer
Professor Oleg G. Shpyrko

2017

The dissertation of Yury Kiselev is approved, and it is acceptable in quality and form for publication on microfilm and electronically:

_____

_____

_____

_____

_____

Chair

University of California, San Diego

2017

DEDICATION

To my parents.

TABLE OF CONTENTS

LIST OF FIGURES

LIST OF TABLES

ACKNOWLEDGEMENTS

I am glad to have a chance to thank my advisor, prof. Daniel Arovas, for his mentorship during my years in UCSD. I appreciate the time my thesis committee members agreed to devote towards evaluating and commenting on my thesis. I thank people whom I met and became friends with in San Diego, especially Margot White, for making my life during these years substantially better. My interest in Physics was ignited already in the high school and number of people since then motivated me to do science in general and physics in particular. It is impossible to thank them all, but I'd like to say thank you here to Mikhail Ivanov, Konstantin Stolbov, Igor Shenderovich, Nikita Gordeev, Leonid Karachinsky, Eougenious Ivchenko, Leonid Golub and Mikhail Glazov.

Chapters 1 contains material from the paper:
Y. Y. Kiselev, S. A. Parameswaran, and D.P. Arovas, "Order and disorder in SU(N) simplex solid antiferromagnets", *Journal of Statistical Mechanics: Theory and Experiment*, 013105, (2016). The dissertation author was the primary investigator and author of this paper.

Chapters 2 contains material from the paper: T. Vojta, J. Crewse, M. Puschmann, D. Arovas, and Y. Kiselev, "Quantum critical behavior of the superfluid-Mott glass transition", *Physical Review B*, 94, 134501, (2016). The dissertation author was a co-author of this paper.

Chapter 3 contains material currently being prepared for submission for publication: Y.Y. Kiselev and D.P. Arovas, "Large-N limit and phase transitions of two-dimensional Sp(N) magnets". The dissertation author was the primary investigator and author of this work.

Chapter 4 contains material currently being prepared for submission for publication: Y.Y. Kiselev and D.P. Arovas, "Two and one-dimensional Floquet

systems". The dissertation author was the primary investigator and author of this work.

VITA

2009	B. Sc. in Applied Physics, St. Petersburg State Polytechnic University, Russia
2011	M. Sc. in Physics, St. Petersburg Academic University, Russia
2017	Ph. D. in Physics, University of California, San Diego, U.S.

PUBLICATIONS

T. Vojta, J. Crewse, M. Puschmann, D. Arovas, and Y. Kiselev, "Quantum critical behavior of the superfluid-Mott glass transition", *Physical Review B*, 94, 134501, (2016).

Y.Y. Kiselev, S.A. Parameswaran, and D.P. Arovas, "Order and disorder in SU(N) simplex solid antiferromagnets", *Journal of Statistical Mechanics: Theory and Experiment*, 013105, (2016).

Y.Y. Kiselev and L.E. Golub, "Optical and photogalvanic properties of graphene superlattices formed by periodic strain", *Physical Review B*, 84, 235440, (2011).

I.I. Novikov, N.Yu. Gordeev, Yu.M. Shernyakov, Y. Y. Kiselev, M.V. Maximov, P.S. Kopev, A. Sharon, R.Duboc, D.B. Arbiv, U. Ben-Ami, V.A. Shchukin, and N.N. Ledentsov, "High-power single mode (>1 W) continuous wave operation of longitudinal photonic band crystal lasers with a narrow vertical beam divergence", *Applied Physics Letters*, 92, 103515, (2008).

ABSTRACT OF THE DISSERTATION

Order And Disorder In Spin Systems

by

Yury Kiselev

Doctor of Philosophy in Physics

University of California, San Diego, 2017

Professor Daniel P. Arovas, Chair

The study of various types of orders and phases of matter in magnetic systems is extremely popular theme in condensed matter physics. Not only frequently applicable in real world, quantum magnetism provides a fruitful and at the same time frequently feasible framework to search for new phases of matter. In this work we study quantum and associated classical phase transitions of spin systems by combinations of numerical and analytical methods.

In Chapter 1 we study quantum paramagnets that are a generalization of antiferromagnetic AKLT [2] construction for the spin group SU(N). We map the so called simplex solid state ansatz wavefunction into a partition function of the

classical system on the same lattice using coherent state representation. Then we study phase transitions of that classical models via classical Monte Carlo methods to determine properties of the original quantum simplex solid state [3].

In Chapter 2 we are interested in the O(2) model in (2+1)-dimensional system with the dilution, i.e. when some sites are removed from the system. This relativistic O(2) model originates from the description of a transition between superfluid and Mott insulator phases. We study critical properties of the transition using a recently invented [4] worm algorithm.

In Chapter 3 we are studying large-N expansion for the symplectic spin group Sp(N). When the original SU(2) spin model proves to be too difficult to be solved, for example at low temperatures, one of the alternative ways is to consider a system based on a more general spin group, for example SU(N) or Sp(N). Results often remain relevant for the original SU(2) group. We are using the mean-field theory approach to find phase transitions associated with the cubic Sp(N) system at large N.

Another fundamental question of interest is how different systems behave when they are periodically driven by some external field. Such systems are called Floquet systems, and we will study them in Chapter 4. We will consider interacting and non-interacting systems, that might have a non-conventional type of ordering, topological order.

Chapter 1

Ordered and disordered ground states of SU(N) simplex solid antiferromagnets

1.1 Introduction

While the SU(2) ferromagnet can be locally understood by classical arguments of locally aligned spins, antiferromagnets are much more quantum in this sense. Minimum energy of two spins is achieved when the two spins form a singlet. This notion led to the idea of 'valence bond solid' (VBS) wavefunctions that first were constructed from spins paired locally into singlets with their neighbors of the lattice. The problem with this construction is that it frequently breaks lattice symmetries – a given spin can form a singlet only with one of its neighbors.

In a landmark paper [5], Affleck, Kennedy, Lieb and Tasaki (AKLT) presented an explicit construction of a family of VBS wavefunctions that did not have such problem. Their construction places several virtual spins 1/2 onto each site of the lattice, and then forms singlets between spins 1/2 on the neighboring sites, see Fig. 1.1. Clearly number of initial spins on each site should divide the lattice coordination number r. The local spin quantum number is $S = \frac{1}{2}Mr$ (so large M means less quantum fluctuations) and each VBS wave function is a ground state of a Hamiltonian which may be written as a sum of local projection operators. The simplest example is the one-dimensional $S = 1$ AKLT chain, whose wavefunction is the nondegenerate ground state (on a ring) of the Hamiltonian $H = \sum_n \boldsymbol{S}_n \cdot \boldsymbol{S}_{n+1} + \frac{1}{3}(\boldsymbol{S}_n \cdot \boldsymbol{S}_{n+1})^2$. This state provided the first exact wavefunction for a system exhibiting a Haldane gap [6, 7]. These isotropic valence bond solid (VBS) states provide a useful paradigm for quantum paramagnets in which both spin and lattice point group symmetries remain unbroken. As noted more recently by Yao and Kivelson [8], the AKLT states are also examples of 'fragile Mott insulators', that cannot be adiabatically connected to a band

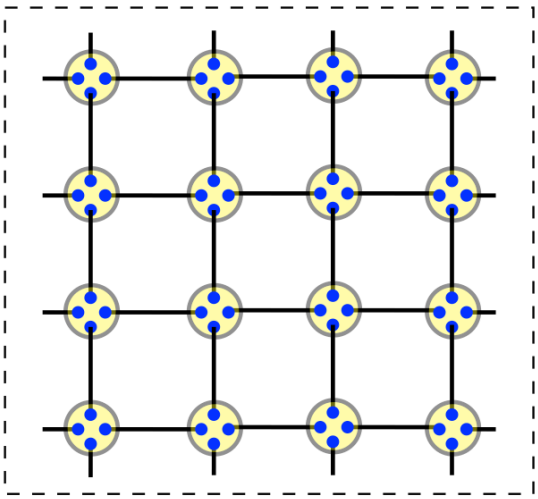

Figure 1.1: AKLT construction on a square lattice, $M = 1$.

insulator while preserving certain point-group symmetries. In dimensions $d > 2$, the VBS states may exhibit long-ranged Néel order if M is sufficiently large.

The AKLT construction is based on application of local singlet bond operators for SU(2) spins. We are going to explore the properties of an extension of the VBS family to SU(N) quantum spins, first discussed by Arovas et al. [9], in which the singlets reside on N-site simplices. These simplex solid models have much in common with their VBS relatives, including featureless $T = 0$ quantum paramagnetic phases, parent Hamiltonians of which are sums of local projectors, nondegenerate ground states regardless of base space topology, area law entanglement, and possibly broken SU(N) symmetry in $d > 2$ dimensions. As with the VBS states, for each lattice $\mathcal{L}$ there is a discrete one-parameter family of models, labeled by an integer M, which together determine the local representation of SU(N). And, similarly, in dimensions $d > 2$ the simplex solids may solidify into a spin crystal, *i.e.* a generalized Néel state, provided M is sufficiently large.

We will consider several examples of simplex solid states, and study

their properties via a combination of methods, including classical Monte Carlo and various analytical methods. The key technical feature which permits such analyses is a mapping, via generalized spin coherent states, of the equal time quantum correlations of the simplex solid wavefunctions to finite temperature correlations of an associated *classical* model on the same lattice – another aspect shared with the VBS states [10]. We will therefore focus on the properties of these classical models, their possible ordered phases, mean field descriptions, and analysis of low-energy effective models. We will find, and explain why, that, unlike the VBS models, some $d > 2$ simplex solids never order for *any* finite value of M, no matter how large.

1.2 Valence bond and Simplex solid states

For each lattice $\mathcal{L}$ there is a family of VBS states indexed by a positive integer M, constructed as follows [5]: First, place Mr spin-$\frac{1}{2}$ objects on each site, where r is the lattice coordination number (we assume $r_i = r$ for all sites i in $\mathcal{L}$). Next, contract the SU(2) indices by forming M singlet bonds on each link of the lattice. Finally, symmetrize over all the SU(2) indices on each site. This last step projects each site spin into the totally symmetric $S = \frac{1}{2}Mr$ representation, *i.e.* a Young tableaux with one row of Mr boxes. The general state $|\Psi(\mathcal{L}, M)\rangle$ is conveniently represented using the Schwinger boson construction [10], where $\boldsymbol{S} = b^\dagger_\mu \boldsymbol{\sigma}_{\mu\nu} b_\nu$ and the total boson number on each site is $b^\dagger_\uparrow b_\uparrow + b^\dagger_\downarrow b_\downarrow = 2S$:

$$\Big|\Psi(\mathcal{L}, M)\Big\rangle = \prod_{\langle ij\rangle \in \mathcal{L}} \left(b^\dagger_{i\uparrow} b^\dagger_{j\downarrow} - b^\dagger_{i\downarrow} b^\dagger_{j\uparrow}\right)^M \Big|0\Big\rangle \,. \tag{1.1}$$

Since the bond operator $\phi^\dagger_{ij} = \varepsilon^{\mu\nu} b^\dagger_{i\mu} b^\dagger_{j\nu}$ transforms as an SU(2) singlet, M of the bosons at site i are fully entangled in a singlet state with M bosons on site j, so that the maximum value of the total spin J_{ij} is $2S - M$, and thus $|\Psi(\mathcal{L}, M)\rangle$ is an exact zero energy ground state for any Hamiltonian of the form $H = \sum_{\langle ij \rangle} \sum_{J=2S-M+1}^{2S} V_J P_J(ij)$, where $V_J > 0$ are pseudopotentials and $P_J(ij)$ is the projector onto total spin J for the link (ij).

Many properties of $|\Psi(\mathcal{L}, M)\rangle$ may be gleaned from its coherent state representation [10], $\Psi_{\mathcal{L},M}[z] = \prod_{\langle ij \rangle \in \mathcal{L}} \left(\epsilon^{\mu\nu} z_{i\mu} z_{j\nu} \right)^M$, where for each site i, z_i is a rank-2 spinor with $z_i^\dagger z_i = 1$ and $z_i \equiv e^{i\alpha} z_i$, *i.e.* an element of the complex projective space $\mathrm{CP}^1 \cong \mathrm{S}^2$. In particular, one has $\left| \Psi_{\mathcal{L},M}[z] \right|^2 = e^{-H_{\mathrm{cl}}/T}$, where

$$H_{\mathrm{cl}} = - \sum_{\langle ij \rangle \in \mathcal{L}} \ln \left(\frac{1 - \hat{\boldsymbol{n}}_i \cdot \hat{\boldsymbol{n}}_j}{2} \right), \tag{1.2}$$

with $\hat{\boldsymbol{n}}_i = z_i^\dagger \boldsymbol{\sigma} z_i \in \mathrm{S}^2$ is a unit vector, is the Hamiltonian for a classical O(3) antiferromagnet on the same lattice $\mathcal{L}$, and $T = 1/M$ is a fictitious temperature. This is analogous to Laughlin's 'plasma analogy' for the fractional quantum Hall effect, and we may similarly use well-known results in classical statistical mechanics to deduce properties of the state described by $|\Psi(\mathcal{L}, M)\rangle$. Specifically, we may invoke the Hohenberg-Mermin-Wagner theorem to conclude that all AKLT states in dimensions $d \leq 2$ lack long-range magnetic order since they correspond to a classical O(3) system at finite temperature on the same lattice[1]. For $d > 2$, a mean-field analysis [5, 11] suggests that the AKLT states on bipartite lattices possess long-ranged two sublattice antiferromagnetic order for $T < T_{\mathrm{c}}^{\mathrm{MF}} = \frac{1}{3} r$, *i.e.* $M > M_{\mathrm{c}}^{\mathrm{MF}} = 3r^{-1}$. Since the minimum possible value for M is $M = 1$, the

[1] Note however that in two dimensions there remains the possibility of broken point-group symmetry without spin order – as these are discrete symmetries, their breaking is *not* forbidden in $d = 2$.

mean field analysis suggests that all such $d = 3$ models, where $r > 3$, are Neel ordered. However, mean field theory famously fails to account for fluctuation effects which drive T_c lower – hence M_c higher – for instance, ref. [11] found, using classical Monte Carlo simulations of the corresponding classical O(3) model, that the $S = 2$ (*i.e.* $M = 1$) AKLT state on the diamond lattice ($r = 4$) is quantum-disordered. Ref. [11] also showed that AKLT states on the frustrated pyrochlore lattice were quantum-disordered for $S \leq 15$ (at least). A subsequent extension of the AKLT model to locally tree-like graphs – often used to model disordered systems – found AKLT states that exhibit not only long-range order and quantum disorder, but also those that showed spin glass-like order for large values of the singlet parameter and/or the local tree coordination number [12].

Upon enlarging the symmetry group of each spin to SU(N), there are two commonly invoked routes to singlet ground states. The first is to work exclusively with bipartite lattices, and choose the spins on one sublattice to transform according to the (N-dimensional) fundamental representation of SU(N), while those on the other transform according to the (N-dimensional) conjugate representation. One then has $N \otimes \bar{N} = \bullet \oplus \mathrm{adj}$, where $\bullet$ denotes the singlet and adj the $(N^2 - 1)$-dimensional adjoint representation. Proceeding thusly, one can develop a systematic large-N expansion [13, 14]. Note, however, that on bipartite lattices in which the two sublattices are equivalent, most assignments of bond singlets explicitly break either translational or point-group symmetries. (The exceptions typically involve fractionalization, and hence also do not satisfy our desiderata for a featureless quantum paramagnet.)

The second approach, and our exclusive focus in the remainder, is to retain the *same* representation of SU(N) on each site, but to create singlets which extend over a group of N sites. (There is some resemblance with the three-quark

SU(3) color singlet from quantum chromodynamics.) Here we shall explore the ordered and disordered phases in a class of wave functions which generalize the AKLT valence bond construction from SU(2) to SU(N), and from singlets on bonds to those over simplices. The construction and analysis of these "simplex solids" [9] parallels what we know about the AKLT states. If Γ denotes an N site simplex (henceforth an N-simplex) whose sites are labeled $\{i_1,\ldots,i_N\}$, then the operator

$$\phi_\Gamma^\dagger = \varepsilon^{\alpha_1\cdots\alpha_N}\, b^\dagger_{i_1\alpha_1}\cdots b^\dagger_{i_N\alpha_N} \tag{1.3}$$

where $b^\dagger_{i\alpha}$ creates a Schwinger boson of flavor α on site i, transforms as an SU(N) singlet. Generalizing the product over links in the AKLT construction to a product over N-simplices, one arrives at the simplex solid state [9],

$$\left|\Psi(\mathcal{L},M)\right\rangle = \prod_{\Gamma\in\mathcal{L}}\left(\phi_\Gamma^\dagger\right)^M\left|0\right\rangle . \tag{1.4}$$

The resulting local representation of SU(N) is the symmetric one described by a Young table with one row and $p = M\zeta$ boxes, where ζ is the number of simplices to which each site on $\mathcal{L}$ belongs, a generalization of the lattice coordination number r in the case $N = 2$. Projection operator Hamiltonians which render the simplex solid (SS) states exact zero energy ground states were discussed in Ref. [9]. Written in terms of the N-flavors of Schwinger bosons, the SU(N) spin operators take the form $S_{\alpha\beta} = b^\dagger_\alpha b_\beta - \frac{p}{N}\delta_{\alpha\beta}$, and satisfy the commutation relations $\left[S_{\alpha\beta}, S_{\mu\nu}\right] = \delta_{\beta\mu}S_{\alpha\nu} - \delta_{\alpha\nu}S_{\beta\mu}$. As in the AKLT case, while the wave functions (1.4) are certainly exact ground states of local parent Hamiltonians, it is imperative to verify that they do in fact describe featureless paramagnets. In addressing this question, it is once again convenient to employ a coherent-state representation (suitably generalized to SU(N)) so that the answer can be

inferred from analysis of a finite-temperature classical statistical mechanics problem. Using this mapping, described in detail below, in conjunction with the Hohenberg-Mermin-Wagner theorem, we find that although wave functions of the form (1.4) preserve all symmetries in one dimension, once again we must entertain the possibility that they exhibit lattice symmetry-breaking but not magnetic order in $d = 2$, and that both lattice and spin symmetries are spontaneously broken in $d = 3$.

In $d = 2$, we consider the SU(3) simplex solid on the kagome lattice, and using a saddle-point free energy estimate and Monte Carlo simulations of the classical model, we show that it remains quantum-disordered for all M, although there is substantial local sublattice order, corresponding to the so-called $\sqrt{3} \times \sqrt{3}$ structure, for large M (low effective temperature). We then turn to $d = 3$, where we first consider the SU(3) simplex solid on the hyperkagome lattice of corner-sharing triangles. Here we find no discernible structure for any M, leading us to conclude that *all* these simplex solid states are quantum-disordered. We also consider two different simplex solids on the cubic lattice: the SU(4) model with singlets on square plaquettes (that share edges), and the SU(8) version with singlets over cubes (that share faces). While the former exhibits long-range order for all M (in other words, the classical companion model has a continuous transition at $T_c > 1$), the latter exhibits long-range order only for $M \geq 3$, so that the $M = 1, 2$ cases are quantum-disordered.

Before proceeding, we briefly comment on related work. Other generalized Heisenberg models have been discussed in a variety of contexts. Affleck *et al.* [15] investigated extended valence bond solid models with exact ground states which break charge conjugation ($\mathcal{C}$) and lattice translation (t) symmetries, but preserve the product $\mathcal{C}t$. Their construction utilized SU($2N$) spins on each

lattice site, with $N = Mr$ an integer multiple of the lattice coordination number r, with singlet operators extending over $r+1$ sites. Greiter and Rachel [16] constructed SU(N) VBS chains in the fundamental and other representations. Shen [17] and Nussinov and Ortiz [18] developed models with resonating Kekulé ground states described by products of local SU(N) singlets. Plaquette ground states on two-leg ladders were also discussed by Chen *et al.* [19]. VBS states are perhaps the simplest example of matrix product and tensor network constructions [20, 21, 22, 23], and recently the projected entangled pair state (PEPS) construction was extended by Xie *et al.* to one involving projected entangled simplices [24]. We also note that a different generalization to the group Sp(N) permits the development of a large-N expansion for doped and frustrated lattices [25]. Perhaps more relevant to our discussion here, Corboz *et al.* [26] studied SU(3) and SU(4) Heisenberg models on the kagome and checkerboard lattices using the infinite-system generalization of PEPS (iPEPS), concluding that the Hamiltonian *at the Heisenberg point* exhibits $\boldsymbol{q} = 0$ point-group symmetry-breaking [2]. Although their work left open the question of its adiabatic continuity to the exactly solvable point of Ref. [9], this follows immediately, as the order they discuss is inescapable for a simplex solid where the on-site spins are (as in their work) in the fundamental representation of SU(N).

In addition, there are several other examples of featureless quantum paramagnets in the literature, with more general symmetry groups. Besides the aforementioned work by Yao and Kivelson, fragile Mott insulating phases have been recently examined as possible ground states of aromatic molecules in organic chemistry [27]. Quantum paramagnetic analogs of the fragile Mott insu-

[2] Specifically, they argue that the singlets will be formed on one of two inequivalent choices of simplices, such as only on up triangles in the kagome. This is the SU(N) analog of the Majumdar-Ghosh state.

lator for *bosonic* systems endowed with a U(1) symmetry have also been explored, including those with very similar 'plasma mappings' to classical companion models [28, 29]. Finally, recent work (involving two of the present authors) has identified situations when featureless quantum paramagnets are incompatible with crystalline symmetries and $U(1)$ charge conservation [30].

1.3 Classical model and mean field theory

We first briefly review some results of Ref. [9]. Using the SU(N) coherent states $|z\rangle = \frac{1}{\sqrt{p!}}\left(z_\alpha b_\alpha^\dagger\right)^p|0\rangle$, we may again, as with the VBS states, express equal time ground state correlations in the simplex solids in terms of thermal correlations of an associated classical model on the same lattice. One finds $\left|\Psi_{\mathcal{L},M}[z]\right|^2 = e^{-H_{\rm cl}/T}$, with

$$H_{\rm cl} = -\sum_\Gamma \ln|R_\Gamma|^2 \quad , \tag{1.5}$$

where

$$R_\Gamma = \epsilon^{\alpha_1\cdots\alpha_N} z_{i_1\alpha_1}\cdots z_{i_N\alpha_N} \quad , \tag{1.6}$$

where $\{i_1,\ldots,i_N\}$ label the N sites of the simplex Γ. The temperature is again $T = 1/M$. Note that the quantity $|R_\Gamma|$ has the interpretation of a volume spanned by the CP^{N-1} vectors sitting on the vertices of Γ.

To derive a mean field theory, assume that $\mathcal{L}$ is N-partite and is partitioned into N sublattices. (The partitioning may not be the same in all structural unit cells, as the distinction between Figs. 1.2 and 1.3 demonstrates in the case $N = 3$.) For each site i let $\sigma(i) \in \{1,\ldots,N\}$ denote the sublattice to which i belongs. Let $\{\omega_\sigma\}$ denote a set of N mutually orthogonal CP^{N-1} vectors. Setting $z_i = \omega_{\sigma(i)}$ defines a fully ordered state which we will refer to as a Potts state, since it is also

a ground state for a (discrete) N-state Potts antiferromagnet. In any Potts state, $|R_\Gamma| = 1$ for every simplex Γ, hence the ground state energy is $E_0 = 0$.

Next define a real scalar order parameter m, akin to the staggered magnetization in an antiferromagnet, such that

$$\langle Q_{\alpha\beta}(i) \rangle = m \left(P^{\sigma(i)}_{\alpha\beta} - \frac{1}{N} \delta_{\alpha\beta} \right) \quad , \tag{1.7}$$

where $Q_{\alpha\beta}(i) = z^*_{i\alpha} z_{i\beta} - \frac{1}{N} \delta_{\alpha\beta}$ is a locally defined traceless symmetric tensor, and where $P^\sigma = |\omega_\sigma\rangle\langle\omega_\sigma|$ is the projector onto ω_σ. The system is isotropic when $m = 0$, while $m = 1$ in the Potts state. One finds that the mean field critical value for $M = 1/T$ is $M_c^{\rm MF} = (N^2 - 1)/\zeta$. Note that for $N = 2$ and $\zeta = r$ we recover the mean field results for the VBS states, *i.e.* $M_c^{\rm MF} = 3/r$. Thus, mean field considerations lead us to expect more possibilities for quantum disordered simplex solids than for the valence bond solids in dimensions $d > 2$, where almost all the VBS states are expected to have two sublattice Neel order on bipartite lattices. One remarkable feature of the SS mean field theory is that it apparently *underestimates* the critical temperature in models where a phase transition occurs, thus overestimating M_c.

Expanding about the fully ordered state, writing

$$z_i = \left(1 - \pi_i^\dagger \pi_i \right)^{1/2} \omega_{\sigma(i)} + \pi_i \quad , \tag{1.8}$$

where $\omega^\dagger_{\sigma(i)} \pi_i = 0$, the low-temperature classical Hamiltonian is

$$H_{\rm LT} = \sum_\Gamma \sum_{i<j}^N \left| \pi^\dagger_{\Gamma_i} \omega_{\sigma(\Gamma_j)} + \omega^\dagger_{\sigma(\Gamma_i)} \pi_{\Gamma_j} \right|^2 + \mathcal{O}(\pi^3) \quad . \tag{1.9}$$

The field π_i has $(N-1)$ independent complex components. If $g(\varepsilon)$ is the classical

density of states per site, normalized such that $\int_0^\infty d\varepsilon\, g(\varepsilon) = 1$, then

$$\langle \pi_i^\dagger \pi_i \rangle = (N-1)\, T \int_0^\infty \frac{d\varepsilon}{\varepsilon}\, g(\varepsilon) \quad . \tag{1.10}$$

Another expression estimating $T_{\rm c}$ is obtained by setting $\langle \pi_i^\dagger \pi_i \rangle = 1$, beyond which point the fixed length constraint $z_i^\dagger z_1 = 1$ is violated, *i.e.* the low temperature fluctuations of the π field are too large. In contrast to the mean field expression for the critical temperature, $T_{\rm c} = \zeta/(N^2-1)$, value of $T_{\rm c}$ as determined from this criterion depends on the nature of the putative ordered phase, and moreover it vanishes if $\int_0^\infty d\varepsilon\, \varepsilon^{-1}\, g(\varepsilon)$ diverges.

1.3.1 Counting degrees of freedom

For our models, which are invariant under global U(N) rotations, each site hosts a CP^{N-1} vector, with $2(N-1)$ real degrees of freedom (DOF). Thus, per N-simplex, there are $2N(N-1)$ degrees of freedom. The group U(N) has N^2 generators, N of which are diagonal. These diagonal generators act on the spins by multiplying each of the ω_σ by a phase, which has no consequence in CP^{N-1}. Therefore there are only $N(N-1)$ independent generators to account for. Subtracting this number from the number of DOF per simplex, we conclude that, in a Potts state, each simplex satisfies $N(N-1)$ constraints. If our lattice consists of K corner-sharing simplices, then there are $KN(N-1)$ total (real) degrees of freedom: $2N(N-1)$ DOF per simplex times K simplices, and multiplied by $\frac{1}{2}$ since each site is shared by two simplices. There are an equal number of constraints. Thus, the naïve Maxwellian dimension of the ground state manifold is $D_{\rm M} = 0$. However, as we shall see below, we really have $D \geq 0$, and in some

situations, such as for the kagome and hyperkagome models discussed below, $D > 0$. If the number of zero modes is subextensive, the $T = 0$ heat capacity per site should be $C(0) = N - 1$ by equipartition.

1.4 Monte Carlo Simulations

We simulate the classical companion model via Monte Carlo simulations using a single-spin flip Metropolis algorithm. As mentioned above, our primary interest is in determining the phase diagram of the classical model as a function of the temperature, as this will tell us how the quantum system depends on the discrete parameter $M = 1/T$ (recall that this determines the on-site representation of SU(N) by fixing the number of boxes in the Young diagram in a fully symmetric representation of SU(N)). The classical degrees of freedom, obtained via the coherent-state mapping, are CP^{N-1} spins; in our simulations, each CP^{N-1} spin is represented by an N-dimensional complex unit vector $\vec{z}$. The remaining U(1) local ambiguity is harmless.

Local updates are made by generating an isotropic $\delta\vec{z}$ whose length is distributed according to a Gaussian. The local spin vector is updated to

$$\vec{z}' = \frac{\vec{z} + \delta\vec{z}}{|\vec{z} + \delta\vec{z}|} \quad . \tag{1.11}$$

The standard deviation of the Gaussian distribution is adjusted so that a significant fraction ($\sim 30\%$) of proposed moves are accepted.

In order to obtain independent samples, we simulated N_{chain} independent Markov chains, typically of a length of $\sim 10^5 - 10^6$ Monte Carlo steps per site (MCS). Each chain was initialized with random initial conditions and evolved until the total energy was well-equilibrated, and the initial portions of the chain

before this were discarded. For each chain, we obtained the average values of the various quantities and averaged this across chains to get a single number for each temperature. We estimated the error from the standard deviation of the N_{chain} independent thread averages. This is free of the usual complications of correlated samples inherent in estimating the error from a single chain, and it frees us of the need to compute autocorrelation times to weight our error estimate. Note that in the lowest-temperature samples, we used a relatively modest number of independent chains $N_{\text{chain}} \lesssim 10$, but this was already sufficient to obtain reasonably small error bars.

We analyze two main observables. The first is the heat capacity $C = \text{var}(H_{\text{cl}})/T$, proportional to the square of the RMS energy fluctuations. The second is a generalized structure factor, which is built from an appropriate tensor order parameter,

$$Q_{\alpha\beta}(i) = z^*_{i,\alpha}\, z_{i,\beta} - \frac{1}{N}\,\delta_{\alpha\beta} \quad . \tag{1.12}$$

Note that $\vec{z}_i$ itself cannot be used as an order parameter, because its overall phase is ambiguous. This ambiguity is eliminated in the definition of $Q_{\alpha\beta}(i)$, which is similar to the order parameter of a nematic phase. This tensor has the following properties:

- $\text{Tr}\; Q = 0$
- $\langle\, Q \,\rangle \to 0$ as $T \to \infty$ at all sites
- $\text{Tr}\,(Q^2) = \frac{N-1}{N}$
- $\text{Tr}\,(QQ') = -\frac{1}{N}$ if $z^\dagger z' = 0$.

Thus, in any Potts state, $\text{Tr}\; Q(i)\, Q(j) = -\frac{1}{N}$ for any nearest neighbor pair (ij). A

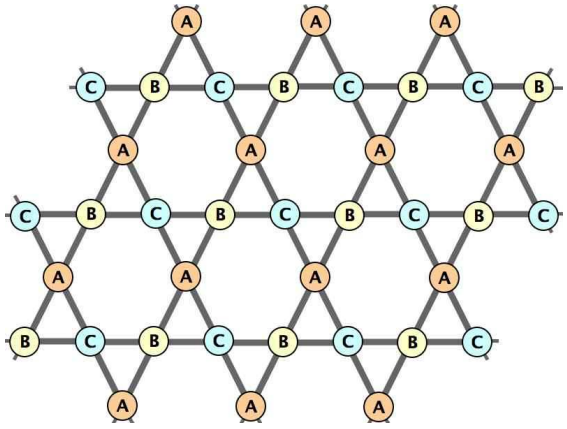

Figure 1.2: The simplest ground state for the kagome structure. A, B, and C represent a set of mutually orthogonal CP^2 vectors.

more detailed measure of order is afforded by the generalized structure factor, which is given by the Hermitian matrix

$$S_{ij}(\boldsymbol{k}) = \frac{1}{\Omega} \sum_{\boldsymbol{R},\boldsymbol{R}'} e^{i\boldsymbol{k}(\boldsymbol{R}-\boldsymbol{R}')} \mathrm{Tr}\Big[Q(\boldsymbol{R},i)\, Q(\boldsymbol{R}',j)\Big]\,, \tag{1.13}$$

where $\boldsymbol{R}$ is a Bravais lattice site, Ω is the total number of the unit cells, and i and j are sublattice indices. The rank of $S_{ij}(\boldsymbol{k})$ is the number of basis vectors in the lattice.

We performed two main tests of the Monte Carlo code. The first (standard) test was to reproduce well-known results: specifically, we recovered the critical temperature $T_c \simeq 0.69$ of the classical cubic lattice O(3) Heisenberg model [31]. Our second concern is more unusual: namely, whether the Metropolis algorithm is sufficiently ergodic to generate a phase transition for a classical system governed by the unusual interaction relevant to simplex solid models: for instance, for a three-site simplex (ijk) we have the interaction $u_{ijk} = -2\ln V_{ijk}$, where $V_{ijk} = |\epsilon^{\mu\nu\lambda} z_{i,\mu}\, z_{j,\nu}\, z_{k,\lambda}|$, is the internal volume of the triple (ijk). In order to ensure that the *absence* of a transition on a more complicated lattice is not simply

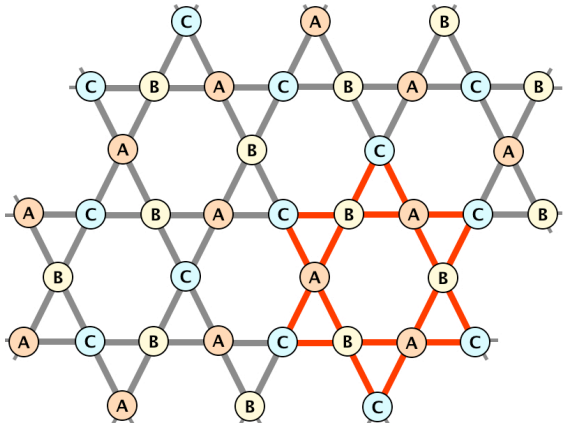

Figure 1.3: The $\sqrt{3} \times \sqrt{3}$ kagome ground state supports an extensive number of zero-energy fluctuation modes. A, B, and C represent a set of mutually orthogonal CP^2 vectors. The red Star of David unit is used to analyze local zero modes.

an artefact of our simulations, it is important to verify that such an interaction can indeed lead to a phase transition in a simple model system. To that end, we investigated a simple SU(3)-invariant model on a simple cubic lattice, with

$$H = -2 \sum_{\boldsymbol{R}} \sum_{\mu=1}^{3} \ln V(\boldsymbol{R} - \hat{\boldsymbol{e}}_\mu, \boldsymbol{R}, \boldsymbol{R} + \hat{\boldsymbol{e}}_\mu) \quad . \tag{1.14}$$

As this is an unfrustrated lattice, with a finite set of broken-symmetry global energy minima (up to global SU(3) rotations) and in three dimensions where fluctuation effects should not destabilize order, it is reasonable to expect a finite-temperature transition in this model. Indeed, we find a transition at $T \simeq 1.25$ or $M \simeq 0.8$, visible in both heat capacity and structure factor calculations. Armed with this reassuring result, we now turn our attention to several specific examples in two and three dimensions.

1.5 SU(3) simplex solid on the kagome lattice

As our first example, we consider the SU(3) model on the kagome lattice. The elementary simplices of this lattice are triangles, and $H_{\rm cl}$ describes a classical model of CP^2 spins with three-body interactions, *viz.*

$$H_{cl} = -\sum_{\Gamma} \ln \left| \epsilon^{\alpha_1 \alpha_2 \alpha_3} z_{\Gamma_1,\alpha_1} z_{\Gamma_2,\alpha_2} z_{\Gamma_3,\alpha_3} \right|^2 , \tag{1.15}$$

where Γ_i are the vertices of the elementary triangle Γ. The structure factor $S_{ij}(\boldsymbol{k})$ is then a 3×3 matrix-valued function of $\boldsymbol{k}$.

In any ground state, each triangle is fully satisfied, with $|R_\Gamma| = 1$. One such ground state is the so-called $\boldsymbol{q} = 0$ structure, which is a Potts state with

$$\omega_{\rm A} = \begin{pmatrix} 1 \\ 0 \\ 0 \end{pmatrix} \quad , \quad \omega_{\rm B} = \begin{pmatrix} 0 \\ 1 \\ 0 \end{pmatrix} \quad , \quad \omega_{\rm C} = \begin{pmatrix} 0 \\ 0 \\ 1 \end{pmatrix}$$

assigned to each of the three sublattices of the tripartite kagome structure. The structure factor is given by

$$S_{ij}(\boldsymbol{k}) = \left(\delta_{ij} - \tfrac{1}{3} \right) \cdot \Omega \, \delta_{\boldsymbol{k},0} \quad . \tag{1.16}$$

Another Potts ground state is the $\sqrt{3} \times \sqrt{3}$ structure, depicted in Fig. 1.3, which has a nine site unit cell consisting of three elementary triangles. The

structure factor is then

$$S_{ij}(\boldsymbol{k}) = \frac{\Omega}{3}\begin{pmatrix} 1 & \omega^2 & \omega \\ \omega & 1 & \omega^2 \\ \omega^2 & \omega & 1 \end{pmatrix}\delta_{\boldsymbol{k},\boldsymbol{K}} + \frac{\Omega}{3}\begin{pmatrix} 1 & \omega & \omega^2 \\ \omega^2 & 1 & \omega \\ \omega & \omega^2 & 1 \end{pmatrix}\delta_{\boldsymbol{k},\boldsymbol{K}'} \tag{1.17}$$

where $\omega = e^{2\pi i/3}$ and $\boldsymbol{K}$ and $\boldsymbol{K}'$ are the two inequivalent Brillouin zone corners.

We emphasize that the Potts states do not exhaust all possible ground states, because for some spin configurations, certain collective local spin rotations are possible without changing the total energy. The number of such zero modes can even be extensive [32]. In the case of the SU(4) model on the cubic lattice, to be discussed below, there are only finitely many soft modes, and we observe a finite temperature phase transition.

Consider now the zero-energy fluctuations for the $\boldsymbol{q} = 0$ structure. Six of them are global SU(3) rotations, while the others may be constructed as follows. Identify A, B, and C spin sublattices by different colors. There are three types of dual-colored lines in this structure (see Fig. 1.2): ABAB, BCBC, and CACA. The spins along each of these lines may be rotated independently around ω_σ axis corresponding to the third color. This is a source of zero modes: each line provides two zero modes, but total number of zero modes in this structure is still sub-extensive, scaling as $\Omega^{1/2}$.

For the $\sqrt{3}\times\sqrt{3}$ structure of Fig. 1.3, there is an extensive set of zero modes. Consider the case of a single Star of David from this structure, depicted in red in the figure. The internal hexagon is a six-site loop surrounded by six external spins. If the loop spins belong to the plane spanned by vectors $z_{\rm A}$ and $z_{\rm B}$ while the external spins are all $z_{\rm C}$, there is a local zero-energy mode associated with the hexagon which rotates $z_{\rm A}$ and $z_{\rm B}$ about $z_{\rm C}$, while keeping all three spins

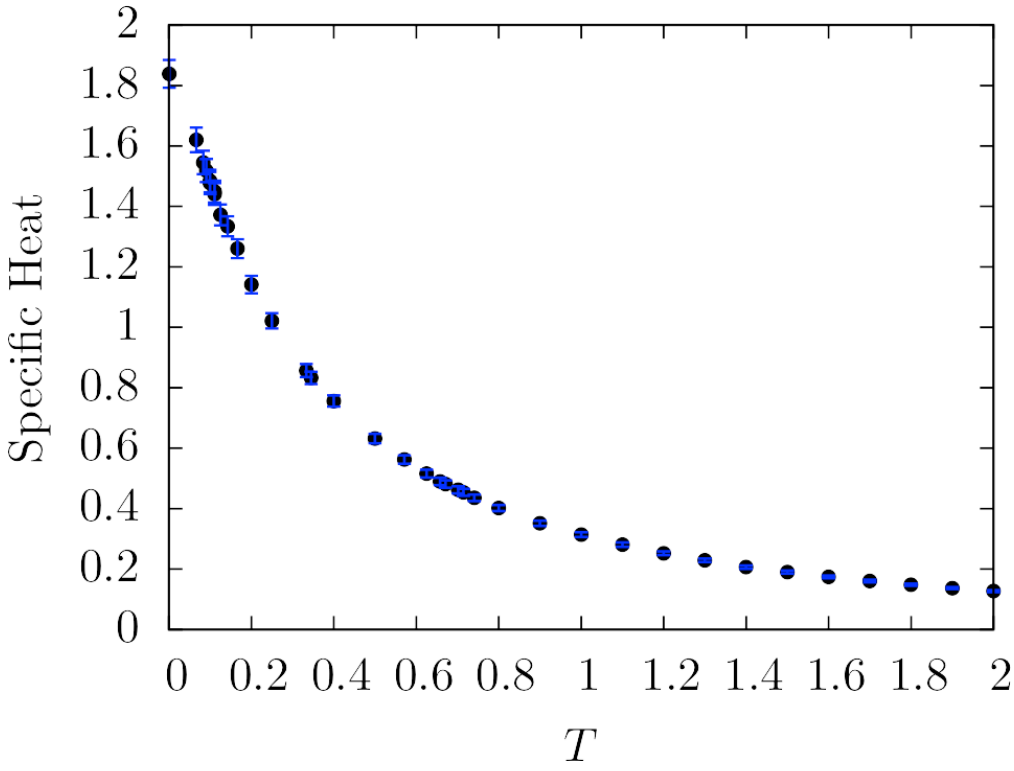

Figure 1.4: Specific heat per site *versus* temperature for the kagome structure with $N = 1296$ sites.

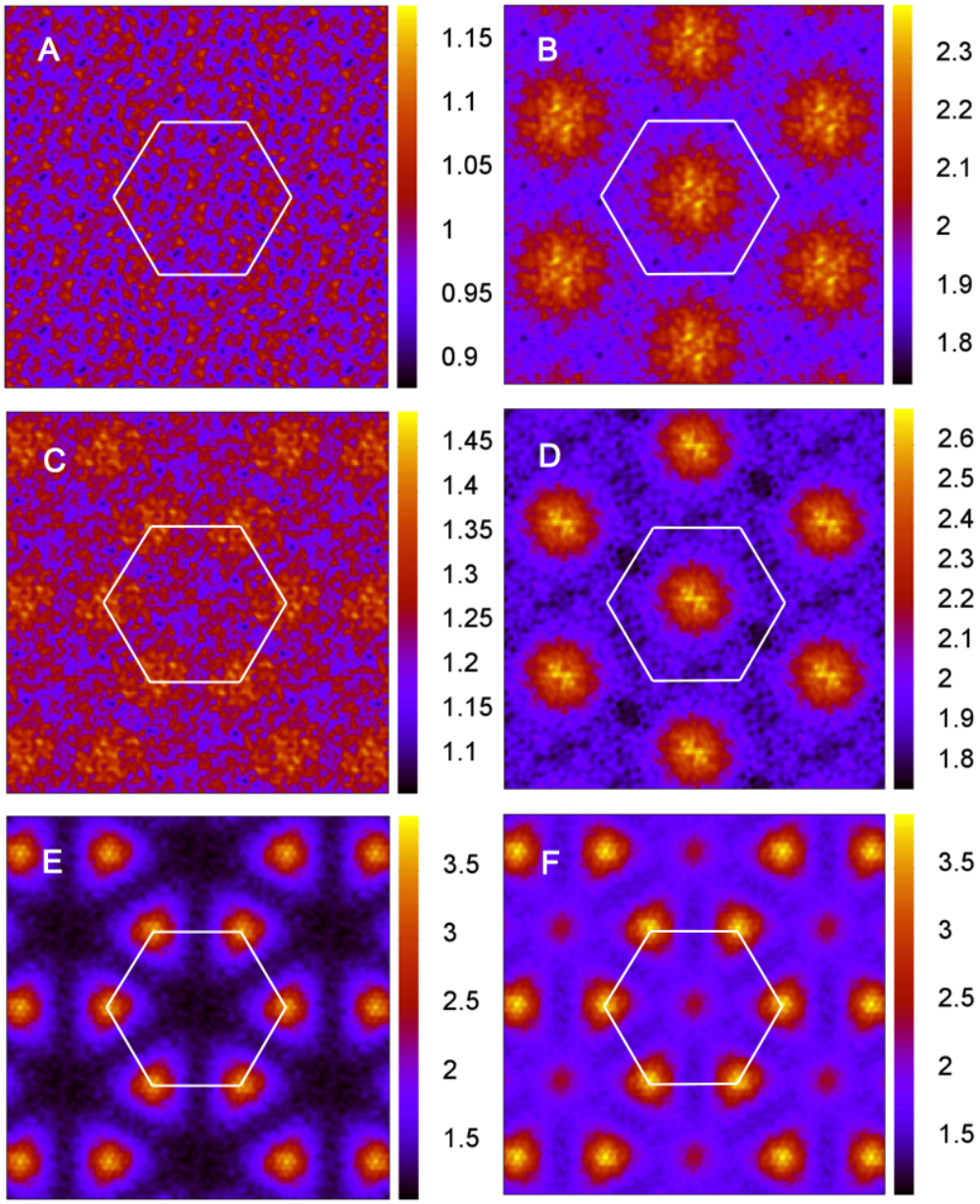

Figure 1.5: Structure factors for the SU(3) kagome lattice model. Left (A,C,E): largest eigenvalue, Right (B,D,F): sum of all eigenvalues. A,B correspond to $M = 2$ (high temperature); C,D to $M = 5$; E,F (low temperature) to $M = 20$.

mutually orthogonal. For a single six-site loop with six additional vertices this type of fluctuation coincides with the global rotation, but in the lattice we can rotate each of the loops independently. This leads to the extensive number of zero modes, which increases the entropy. Fluctuations about the Potts state yield a heat capacity of $C = \frac{16}{9} \approx 1.78$ per site. The counting of modes is as follows. There are four quadratic modes per site. Any individual hexagon, however, can be rotated by a local U(2) matrix in the subspace perpendicular to the direction set by its surrounding spins (*e.g.*, an AB hexagon can be rotated about the C direction). There are two independent real variables associated with such a rotation. (For an AB hexagon, the A sites are orthogonal to the C direction, hence $z_{\rm A}$ is specified by two complex numbers, plus the constraint of $z_{\rm A}^\dagger z_{\rm A} = 1$ and the equivalence under $z_{\rm A} \to e^{i\alpha} z_{\rm A}$.) Subtracting out the zero modes, we find the heat capacity per site would then be $C(0) = \frac{1}{2} \times \left(4 - \frac{2}{3}\right) = \frac{5}{3}$. However, we have subtracted too much. Only one third of the hexagons support independent zero modes (the AB hexagons, say). The remaining two thirds are not independent and will contribute at quartic order in the energy expansion. The specific heat contribution from these quartic modes is then $\frac{1}{4} \times \frac{2}{3} \times \frac{2}{3} = \frac{1}{9}$. Thus, we expect $C(0) = \frac{16}{9}$. This analysis of the zero modes in both structures follows that for the O(3) Heisenberg antiferromagnet on the kagome lattice [33]. As in the O(3) case, the low temperature entropy selects configurations which are locally close to the $\sqrt{3} \times \sqrt{3}$ structure. This order by disorder (OBD) mechanism was shown in Ref. [9] by invoking a global length constraint which turns the low temperature Hamiltonian of eqn. 1.9 into a spherical model, introducing a single Lagrange multiplier λ to enforce $|\chi|^2 + \frac{1}{\Omega} \sum_i \langle \pi_i^\dagger \pi_i \rangle = 1$, where χ plays the role of

a condensate amplitude. The free energy per site is then

$$f = -\lambda + \lambda|\chi|^2 + (N-1)\,T \int_0^\infty d\varepsilon\; g(\varepsilon)\; \ln\left(\frac{\varepsilon+\lambda}{T}\right) \quad . \tag{1.18}$$

Extremizing with respect to λ yields the saddle point equation, and the OBD selection follows from a consideration of saddle-point free energies of the $\boldsymbol{q} = 0$ and $\sqrt{3}\times\sqrt{3}$ states.

We now turn to the results of our Monte Carlo simulations. The heat capacity $C(T)$ per site is shown in Fig. 1.4. We find $C(T)$ exhibits no singularities at any finite temperature and remains finite at zero temperature. Thus, there is no phase transition down to $T = 0$. Note that while the Hohenberg-Mermin-Wagner theorem forbids the breaking of the continuous SU(3) symmetry at finite temperatures (since the classical Hamiltonian $H_{\rm cl}$ is that of a two-dimensional system with finite-range interactions) it leaves open the possibility of a transition due to breaking a discrete lattice symmetry. That such a transition does not occur – as evinced by the absence of any specific heat singularities – is a nontrivial result of these simulations. From equipartition, we should expect $C = 2$ if all freedoms appear quadratically in the effective low energy Hamiltonian. Instead, we find $C(0) = 1.84 \pm 0.03$. The fact that the heat capacity is significantly lower than 2 suggests that there is an extensive number of zero modes or or other soft modes.

Although the absence of any phase transition in the specific heat data suggests that there is no true long-range order in the kagome system even at $T = 0$, it leaves open the question of whether there is some form of incipient local order in the system as $T \to 0$. To further investigate the local order at low temperatures, we turn to the structure factor $S_{ij}(\boldsymbol{k})$. Recall that this is a

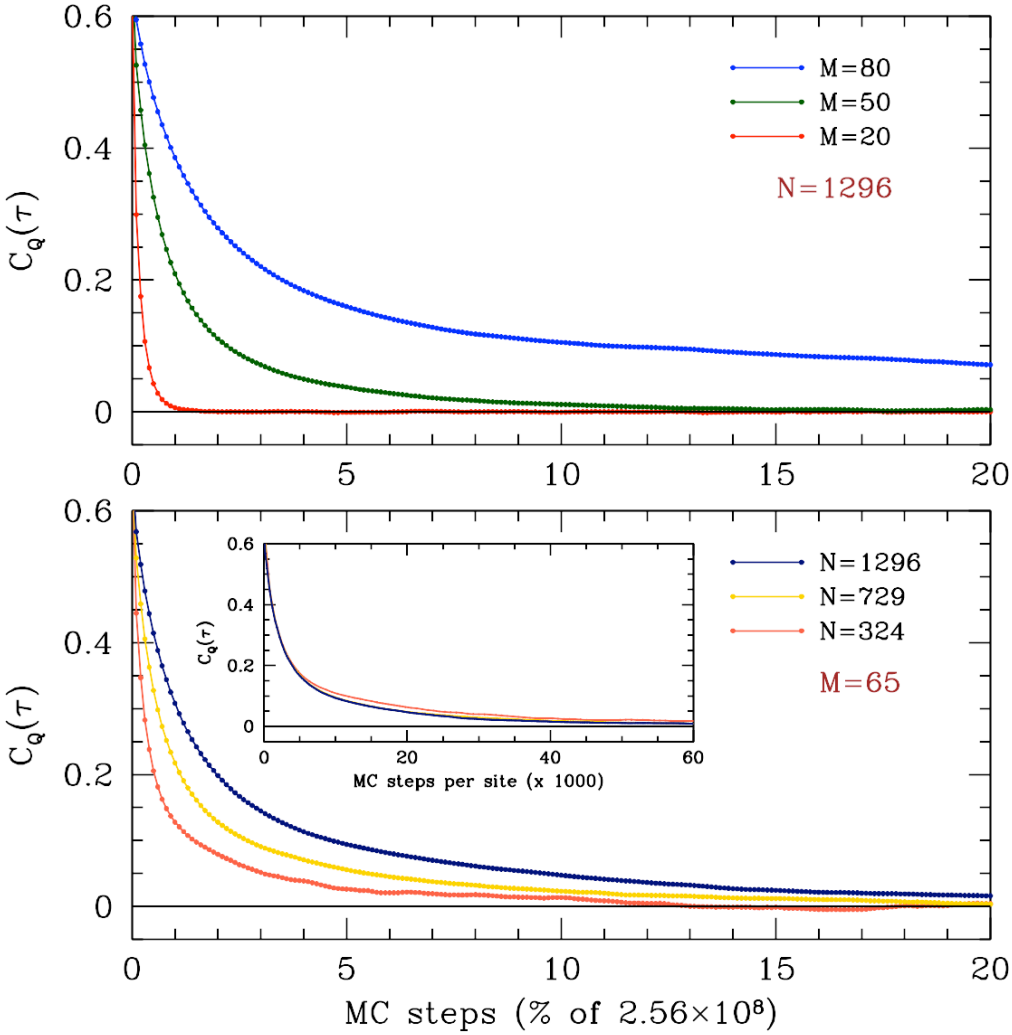

Figure 1.6: Autocorrelation function $C_Q(\tau)$ *vs.* MC time for the SU(3) model on the kagome lattice. Upper panel: Behavior for $N = 1296$ site system at inverse temperatures $M = 20, 50$ and 80. Bottom panel: $M = 65$ data for different sized systems.

3×3 matrix for the kagome lattice, and we have focused our attention on the eigenvalue of maximum amplitude as well as the trace of this matrix. Our Monte Carlo results for these quantities are plotted in Fig. 1.5 for the kagome lattice that consisted of $N = 1296$ sites. White hexagon on the pictures indicates the border of Brillouin zone. At high temperatures, we find the only detectable structure has the same periodicity as the lattice, with $\mathrm{Tr}\, S(\boldsymbol{k})$ exhibiting a peak at the center of the Brillouin zone. Upon lowering temperature, one can see that additional structure emerges, and the peak shifts to the Brillouin zone corners $\boldsymbol{K}$ and $\boldsymbol{K}'$, corresponding to the $\sqrt{3} \times \sqrt{3}$ structure. The width of the structure factor peaks remains finite down to $T = 0$, and there are no true Bragg peaks. The heat capacity of the ideal $\sqrt{3} \times \sqrt{3}$ structure is somewhat lower than the heat capacity obtained from Monte Carlo simulations.

Further insight on the nature of the low-temperature state of the kagome simplex solid is afforded by studying the autocorrelation function $C_Q(\tau' - \tau) = \langle \mathrm{Tr}\left[Q(i,\tau)\, Q(i,\tau')\right]\rangle$, where additional averaging was performed over the starting time τ and the site index i.

Fig. 1.6 shows the autocorrelation function $C_Q(\tau)$ versus Monte Carlo time for the SU(3) model on the kagome lattice. The inset there shows $C_Q(\tau)$ versus Monte Carlo steps per site. The overlap for different N values indicates size-independence of the results. As is clear from Fig. 1.6, the autocorrelator vanishes for $|\tau' - \tau| \to \infty$, consistent with a lack of long-range order. For larger M (smaller T), the dynamics slow down, consistent with the dominance of the local $\sqrt{3} \times \sqrt{3}$ pattern in the low-temperature structure factor.

1.6 Three-dimensional lattices

1.6.1 SU(3) simplex solid on the hyperkagome lattice

We embark on our analysis of three-dimensional lattices by considering the analog of the kagome in three dimensions: the imaginatively-named hyperkagome lattice (Fig. 1.7). This is a three-dimensional fourfold coordinated lattice consisting of loosely-connected triangles. The crystal structure is simple cubic, with a 12-site basis. It may be described as a depleted pyrochlore structure, where one site per pyrochlore tetrahedron is removed. With triangular simplices, we again have the Hamiltonian of eqn. 1.15, but here owing to the increased dimensionality, we might expect that ordered states remain relatively stable to fluctuation effects.

There is a vast number of ground states of the SU(3) simplex solid model on the hyperkagome lattice. We first consider the simplest ones, Potts states, where three mutually orthogonal CP^2 vectors $\omega_{\mathrm{A,B,C}}$ are assigned to the lattice sites such that the resulting arrangement is a ground state, where the volume of each triangle (ijk), $|R_\Gamma| = |\epsilon^{\alpha\beta\gamma} z_{i,\alpha} z_{j,\beta} z_{k,\gamma}|$ is maximized, *i.e.* $|R_\Gamma| = 1$.

The simplest Potts ground state will have the same periodicity as the lattice ($\boldsymbol{q} = 0$), with its 12 site unit cell. Computer enumeration reveals that there are two inequivalent $\boldsymbol{q} = 0$ structures, one of which is depicted in the top panel of Fig. 1.9. Potts ground states with larger unit cells are also possible, and an example of a Potts state with a 36 site unit cell is shown in the bottom panel of the figure. Such structures are analogs of $\sqrt{3} \times \sqrt{3}$ structure on the kagome lattice, discussed in the previous section.

Monte Carlo simulations of H_{cl} on the hyperkagome lattice show no cusp in $C(T)$, suggesting $T_{\mathrm{c}} = 0$ (Fig. 1.8). In contrast to the kagome, structure factor

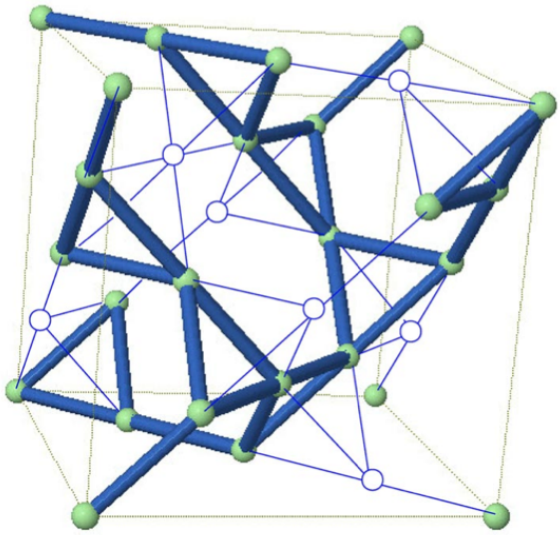

Figure 1.7: The hyperkagome structure (from Ref. [1]).

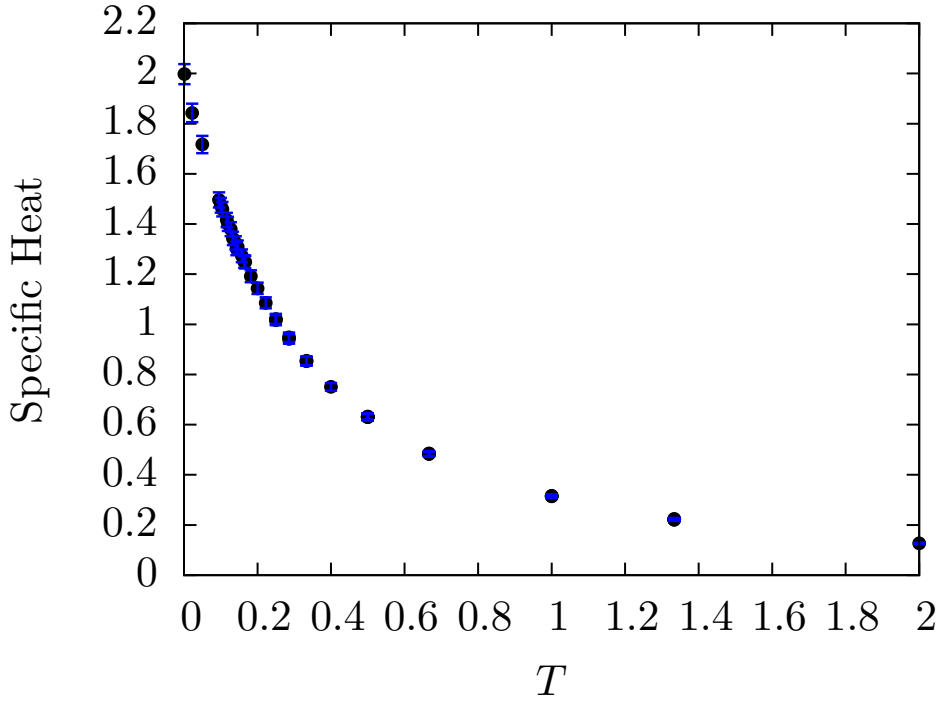

Figure 1.8: Specific heat for the SU(3) model on the hyperkagome lattice with $N = 2592$ sites.

measurements exhibit a diffuse pattern spread throughout the Brillouin zone and are insufficient to show which low temperature structure is preferred (Fig. 1.11).

The six-site loops in the 2D kagome lattice have an analog in the 3D hyperkagome structure, which contains ten-site loops. For the (2D) kagome model, the six-site loops support zero modes in the $\sqrt{3}\times\sqrt{3}$ Potts state. There is an analog of this degeneracy in the (3D) hyperkagome model, where the corresponding Potts state features a 36-site unit cell, mentioned above and depicted in Fig. 1.9. The zero mode corresponds to a SU(3) rotation of all CP^2 spins along a 10-site loop (thick line in the figure), about a common axis. This is possible because all the spins along the loop lie in a common CP^2 plane, forming an ABAB$\cdots$ Potts configuration. A computer enumeration finds that there are 12 distinct such 10-site loops associated with each (12-site) unit cell. If the hyperkagome emulates the kagome, we expect that owing to the abundance of zero modes, structures with such loops will dominate the low-temperature dynamics of $H_{\rm cl}$.

In order to characterize the structure revealed by our Monte Carlo simulations, it is convenient to first define a series of 'loop statistics' measures that serve as proxies for the local correlations of the spins. As before, we define the volume for the triple of sites (i,j,k) as

$$V(i,j,k) = \left|\epsilon^{\mu\nu\lambda} z_{i,\mu}\, z_{j,\nu}\, z_{k,\lambda}\right| \quad , \tag{1.19}$$

i.e. $V(i,j,k) = |R_\Gamma|$ (see eqn. 1.6), where Γ denotes a triangle with vertices (i,j,k). The value of $V^2(i,j,k)$ for different choices of triples in a ten-site loop will serve as our primary statistical measure. Note that $0 \le V(i,j,k) \le 1$, with $V = 0$ if any

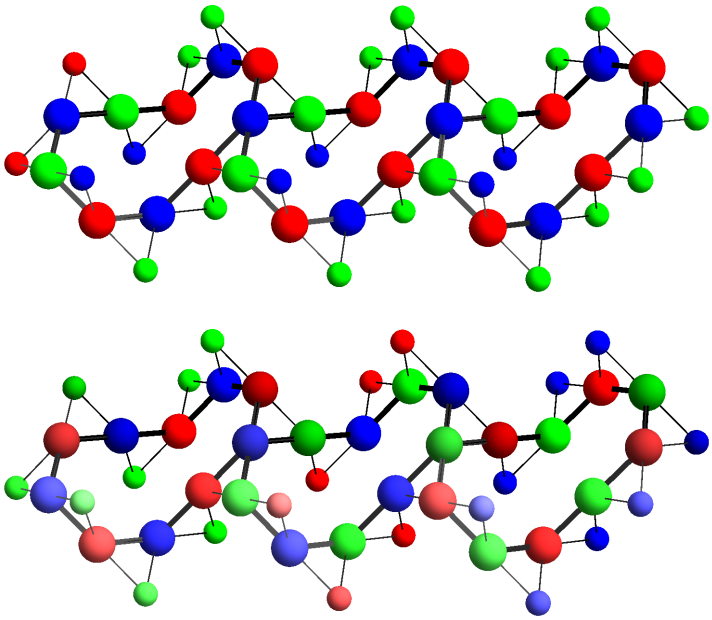

Figure 1.9: Top: Three unit cells, 12 sites each, of the $\boldsymbol{q} = 0$ structure. The 10-site loops do not support any zero modes. Bottom: Unit cell consisting of 36 sites of the structure analogous to $\sqrt{3} \times \sqrt{3}$ in the case of kagome lattice.

two of the CP^2 vectors $\{z_i, z_j, z_k\}$ are parallel, and $V = 1$ if they are all mutually perpendicular. If the CP^2 vectors were completely random from site to site, then the average over three distinct sites would be $\langle V^2(i,j,k)\rangle) = \frac{2}{9}$. For an ABAB$\cdots$ Potts configuration, $V(i,j,k) = 0$ for any three sites along the loop. We then define the loop statistics measures

$$p_{\bullet\bullet\bullet} = \left\langle \tfrac{1}{10} \sum_{i=1}^{10} V^2(i, i+1, i+2) \right\rangle \tag{1.20}$$

$$p_{\bullet\bullet\circ\bullet} = \left\langle \tfrac{1}{10} \sum_{i=1}^{10} V^2(i, i+1, i+3) \right\rangle \tag{1.21}$$

$$p_{\bullet\bullet\circ\circ\bullet} = \left\langle \tfrac{1}{10} \sum_{i=1}^{10} V^2(i, i+1, i+4) \right\rangle \tag{1.22}$$

$$p_{\bullet\circ\bullet\circ\bullet} = \left\langle \tfrac{1}{10} \sum_{i=1}^{10} V^2(i, i+2, i+4) \right\rangle \quad , \tag{1.23}$$

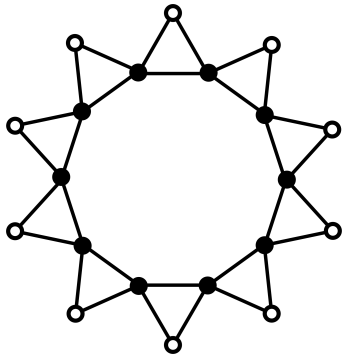

Figure 1.10: A ten site loop surrounded by ten boundary sites.

Table 1.1: 10 site loop statistics in the SU(3) hyperkagome model. A) hyperkagome (lowest $\lambda_{\min}$). B) hyperkagome (lowest $p_{\bullet\circ\bullet\circ\bullet}$). C) 10 sites (uniform boundary). D) 10 sites (no zero mode). E) 20 sites (loop + boundary). Parameter $M = 100$.

SU(3) system	A	B	C	D	E
$p_{\bullet\bullet\bullet}$	0.377 ± 0.004	0.364 ± 0.007	0.0093 ± 0.0006	0.516 ± 0.004	0.488 ± 0.006
$p_{\bullet\bullet\circ\bullet}$	0.2415 ± 0.0008	0.253 ± 0.002	0.0093 ± 0.0006	0.259 ± 0.003	0.253 ± 0.001
$p_{\bullet\bullet\circ\circ\bullet}$	0.305 ± 0.002	0.339 ± 0.003	0.0093 ± 0.0003	0.355 ± 0.007	0.369 ± 0.004
$p_{\bullet\circ\bullet\circ\bullet}$	0.063 ± 0.002	0.043 ± 0.003	0.00025 ± 0.00001	0.138 ± 0.003	0.127 ± 0.005
$\lambda_{\min}$	-0.167 ± 0.001	-0.150 ± 0.002	-0.3296 ± 0.0001	-0.088 ± 0.002	-0.110 ± 0.004
$E/N_\triangle$	0.02945 ± 0.00001	0.02945 ± 0.00001	0.01885 ± 0.00002	0.01984 ± 0.00001	0.029518 ± 0.000003

where the angular brackets denote thermal averages and averages over unit cells.

Another useful diagnostic is to compute the eigenspectrum of the gauge-invariant tensor $Q_{\mu\nu}(i)$ averaged over sites,

$$\overline{Q}_{\mu\nu} \equiv \frac{1}{10} \sum_{i \in \text{loop}} \langle z^*_{i,\mu} z_{i,\nu} \rangle - \tfrac{1}{3}\delta_{\mu\nu} \quad . \tag{1.24}$$

For randomly distributed CP^2 vectors, $\overline{Q} = 0$. If the loop is in the ABAB$\cdots$ Potts configuration, $\overline{Q} = \frac{1}{6} - \frac{1}{2}P_C$, where P_C is the projector onto the C state orthogonal to both A and B. Our final diagnostic is the average energy per triangle, denoted $E/N_\triangle$.

Statistical data for the 10-site loops at inverse temperature $M = 100$ are shown in Table 1.1, where four structures are compared. Each column of the

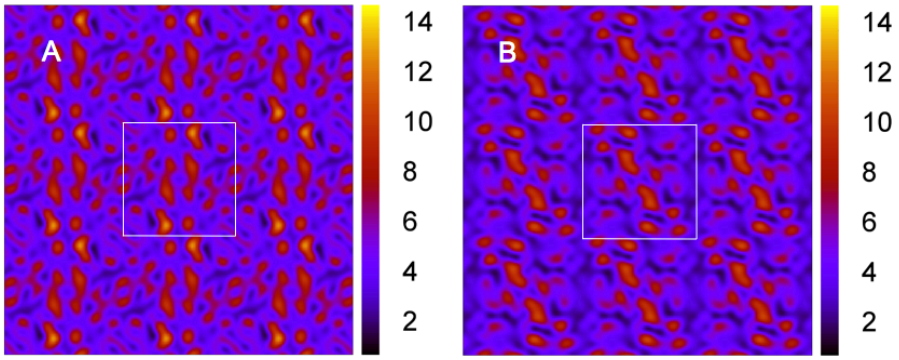

Figure 1.11: Structure factor for the SU(3) hyperkagome model at $T = 0.01$ ($M = 100$). Results show $S(\boldsymbol{k})$ in the (k_x, k_y) plane with $k_z = 0$ (A) and $k_z = \pi/a$ (B) . White lines denote the borders of the Brillouin zone. Number of sites is 6144 (8^3 unit cells).

table refers to a particular class of 10 site loop. The first two columns present Monte Carlo data for a 6144 site lattice (8^3 unit cells) with periodic boundary conditions. Averages are performed over the entire lattice. In the column A, the particular loop among the 12 distinct representatives per unit cell is chosen on the basis of the lowest eigenvalue of $\overline{Q}_{\mu\nu}$. In column B, the representative loop has the lowest value of $p_{\bullet\circ\bullet\circ\bullet}$. In column C, data from a single 10-site loop with a fixed set of boundary spins, as depicted in Fig. 1.10, is presented. In this case the boundary spins are all parallel CP^2 vectors, hence for $T = 0$ the ground state of this ring would be a Potts state of the ABAB$\cdots$ type, and indeed the data are close to what we would predict for such a Potts state, where the internal volume $V(i, j, k)$ vanishes for any triple of sites on the loop, and where the eigenvalues of $\overline{Q}$ are $\left\{-\frac{1}{3}, \frac{1}{6}, \frac{1}{6}\right\}$. Such a configuration exhibits a zero mode, since the loop spins can be continuously rotated about the direction set by the boundary. If we fix the boundary spins such that there is no such zero mode, and average over all such boundary configurations, we obtain the data in column D. Finally, column E presents data for the 20-site system shown in Fig. 1.10, where the boundary spins are also regarded as free.

Our results lead us to conclude that the SU(3) model on the hyperkagome lattice is unlike the planar kagome case in that there it is far from a Potts state, even at low temperatures. There is no thermodynamically significant number of ABAB$\cdots$ ten-site loops, and the statistics of these loops in the hyperkagome structure most closely resemble the results in the last column of Tab. 1.1, corresponding to a single loop with a fluctuating boundary. This is supported by static structure factor data in Fig. 1.11, which shows no discernible peaks. In addition, the heat capacity, shown in Fig. 1.8, tends to the full value of $C(T = 0) = 2N$, corresponding to four quadratic degrees of freedom per site.

1.6.2 SU(4) model on the cubic lattice

Thus far we have considered models with corner-sharing simplices. We now consider a 3D model with edge-sharing simplices. The individual spins are four component objects lying in the space CP^3. These may be combined into singlets using the plaquette operator $\phi^\dagger_\Gamma = \epsilon^{\mu\nu\lambda\rho}\, b^\dagger_{i,\mu}\, b^\dagger_{j,\nu}\, b^\dagger_{k,\lambda}\, b^\dagger_{l,\rho}$, where $(ijkl)$ are the sites of the 4-simplex Γ. On a cubic lattice, M such singlets are placed on each elementary face, so each site is in a fully symmetric representation of SU(4) with $12M$ boxes. Note that two faces may either share a single edge, if they belong to the same cube, or a single site. Again with $T = 1/M$, we have identified a second order phase transition of the corresponding classical system using Monte Carlo simulation. The classical Hamiltonian for the model is

$$H_{\mathrm{cl}} = -\sum_{\Gamma} \ln \left| \epsilon^{\alpha_1\alpha_2\alpha_3\alpha_4}\, z_{\Gamma_1,\alpha_1} z_{\Gamma_2,\alpha_2} z_{\Gamma_3,\alpha_3} z_{\Gamma_4,\alpha_4} \right|^2 , \tag{1.25}$$

where Γ_i are the corners of the elementary square face Γ. An $E_0 = 0$ ground state can be achieved by choosing four mutually orthogonal vectors ω_σ and arranging

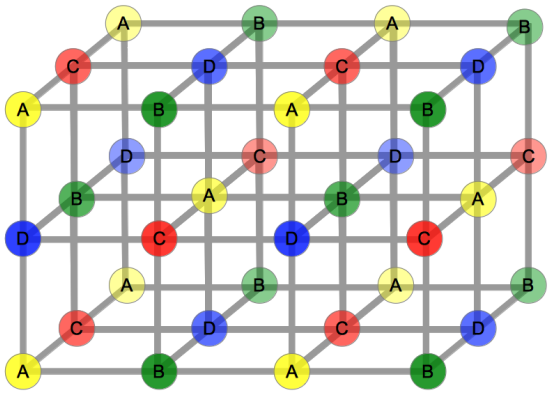

Figure 1.12: Potts ground state of SU(4) classical model on a cubic lattice has a bcc structure.

them in such a way that corners of every face are different vectors from this set. The volume spanned by vectors of every simplex is then $|R_\Gamma| = 1$. This ground state is unique up to a global SU(4) rotation, and has a bcc structure, as shown in Fig. 1.12. Other ground states could be obtained from the Potts state by taking a 1D chain of spins lying along one of the main axes, say ACAC, and rotating these spins around those in the BD plane. We see that number of zero modes is sub-extensive, however.

There is a phase transition to the ordered phase at $T = 1.485 \pm 0.005$. This is confirmed by both heat capacity temperature dependence (Fig. 1.13) and static factor calculations. Our static structure factor calculations prove the spin pattern forms a bcc lattice below the critical temperature (Fig. 1.12 A-B). On the cubic lattice, $S_{ij}(\boldsymbol{k}) = S(\boldsymbol{k})$ is a scalar, and in the Potts state of Fig. 1.12 it is given by

$$\begin{aligned} S(\boldsymbol{k}) &= \frac{1}{\Omega} \sum_{\boldsymbol{R},\boldsymbol{R}'} \mathrm{Tr}\Big[Q(\boldsymbol{R})\, Q(\boldsymbol{R}')\Big] e^{i\boldsymbol{k}\cdot(\boldsymbol{R}-\boldsymbol{R}')} \\ &= \tfrac{1}{4}\Omega \left(\delta_{\boldsymbol{k},\boldsymbol{M}} + \delta_{\boldsymbol{k},\boldsymbol{M}'} + \delta_{\boldsymbol{k},\boldsymbol{M}''}\right) \quad , \end{aligned} \tag{1.26}$$

where $\boldsymbol{M} = (0, \pi, \pi)$, $\boldsymbol{M}' = (\pi, 0, \pi)$, and $\boldsymbol{M}'' = (\pi, \pi, 0)$ are the three inequivalent

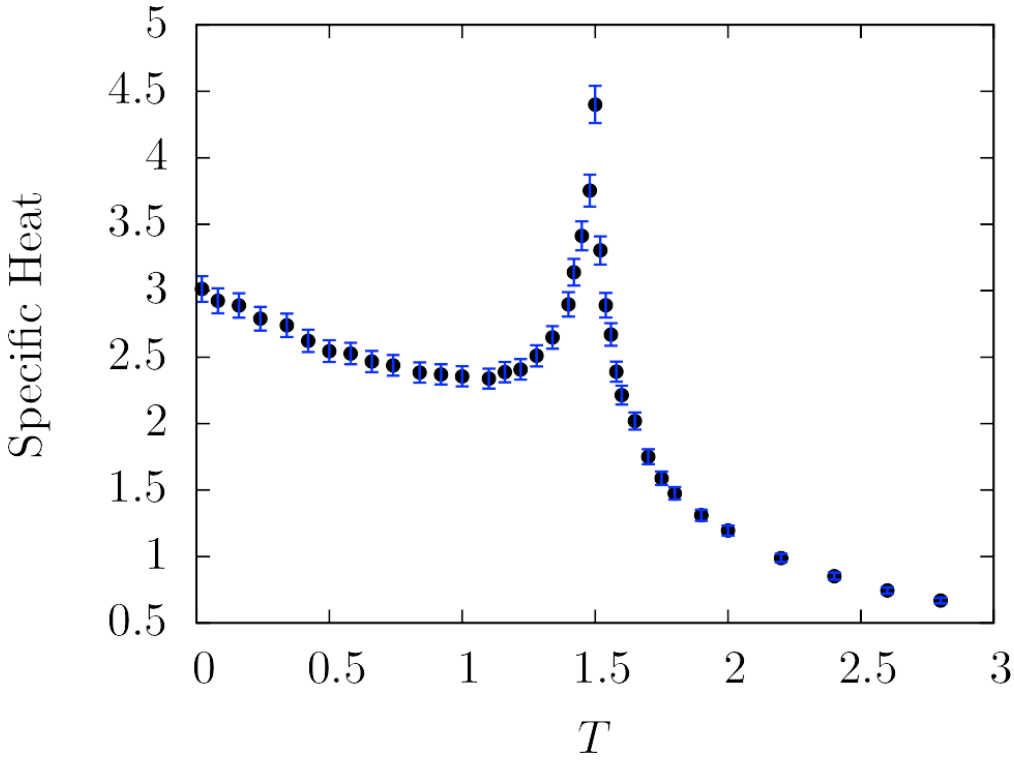

Figure 1.13: Specific heat for SU(4) model on the cubic lattice with $N = 8000$ sites. The phase transition occurs at $T_c \simeq 1.50$.

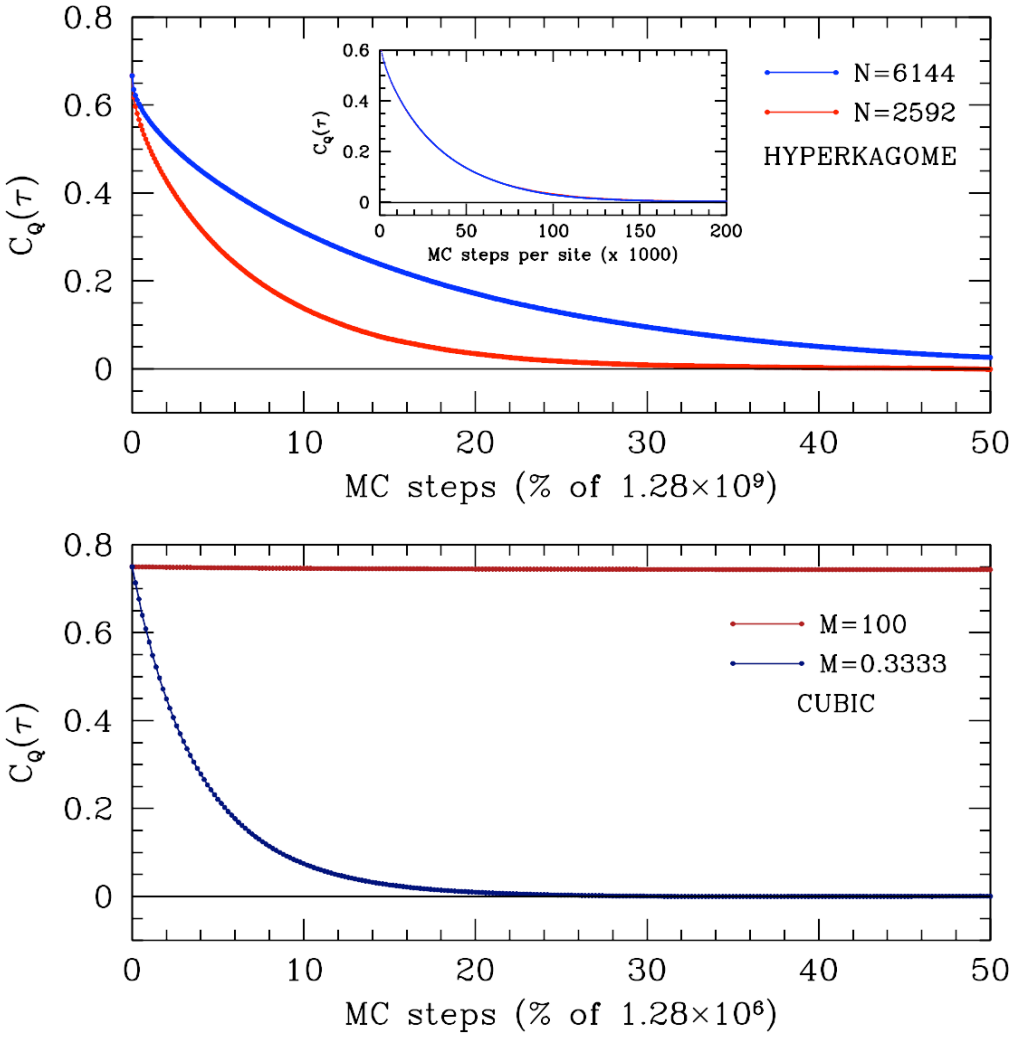

Figure 1.14: Autocorrelation functions $C_Q(\tau)$ *versus* Monte Carlo time for two three-dimensional models. Upper panel: hyperkagome lattice SU(3) model for $N = 2592$ and $N = 6144$ sites. Lower panel: cubic lattice SU(4) model.

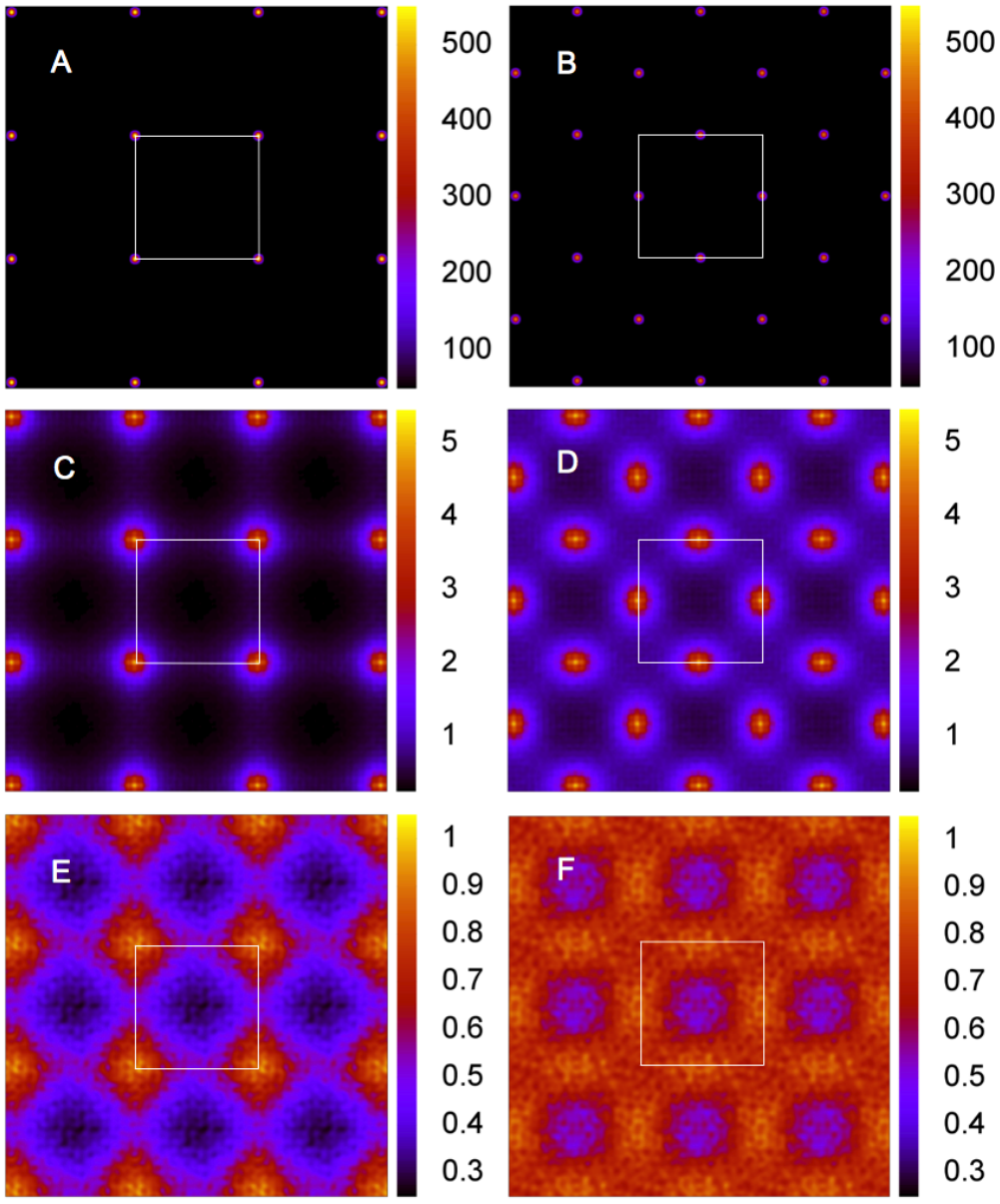

Figure 1.15: Static structure factor for the SU(4) model on the cubic lattice (16^3 sites) as a function of (k_x, k_y) for $k_z = 0$ (A,C,E) and $k_z = \pi$ (B,D,F) and $T = \frac{1}{2}$ (A,B), $T = 1.5$ (C,D), $T = 3$ (E,F). Note the emergence of Bragg peaks for $T < T_c \simeq 1.50$.

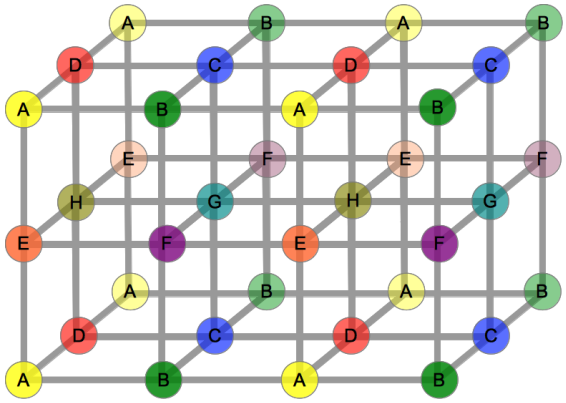

Figure 1.16: A Potts ground state for the SU(8) classical model on the cubic lattice. The magnetic crystal structure is simple cubic.

edge centers of the Brillouin zone, resulting in an edge-centered cubic pattern in reciprocal space. Since $T_c > 1$, we have $M_c < 1$, and since only positive integer M are allowed, we conclude that the SU(4) simplex solid states on the cubic lattice are all ordered. In the mean field theory of Ref. [9], however, one finds $T_c^{\rm MF} = \zeta/(N^2-1)$, where ζ is the number of plaquettes associated with a given site. For the cubic lattice SU(4) model, $\zeta = 12$, whence $T_c^{\rm MF} = \frac{4}{5}$, which lies below the actual T_c. Thus, the mean field theory *underestimates* the critical temperature. In Fig. 1.14 we show the autocorrelators for the SU(3) hyperkagome and SU(4) cubic lattice models. The inset there shows autocorrelation *versus* Monte Carlo steps per site, and the data for the two sizes are overlapping showing that the results are universal. The system is ordered at low temperature ($M = 100$) and disordered at high temperature ($M = 0.3333$). Fig. 1.15 shows the static structure factor and the emergence of Bragg peaks at low temperature.

1.6.3 SU(8) model on the cubic lattice

Finally, we consider a three-dimensional model with face-sharing simplices. On the cubic lattice, with eight species of boson per site, we can construct

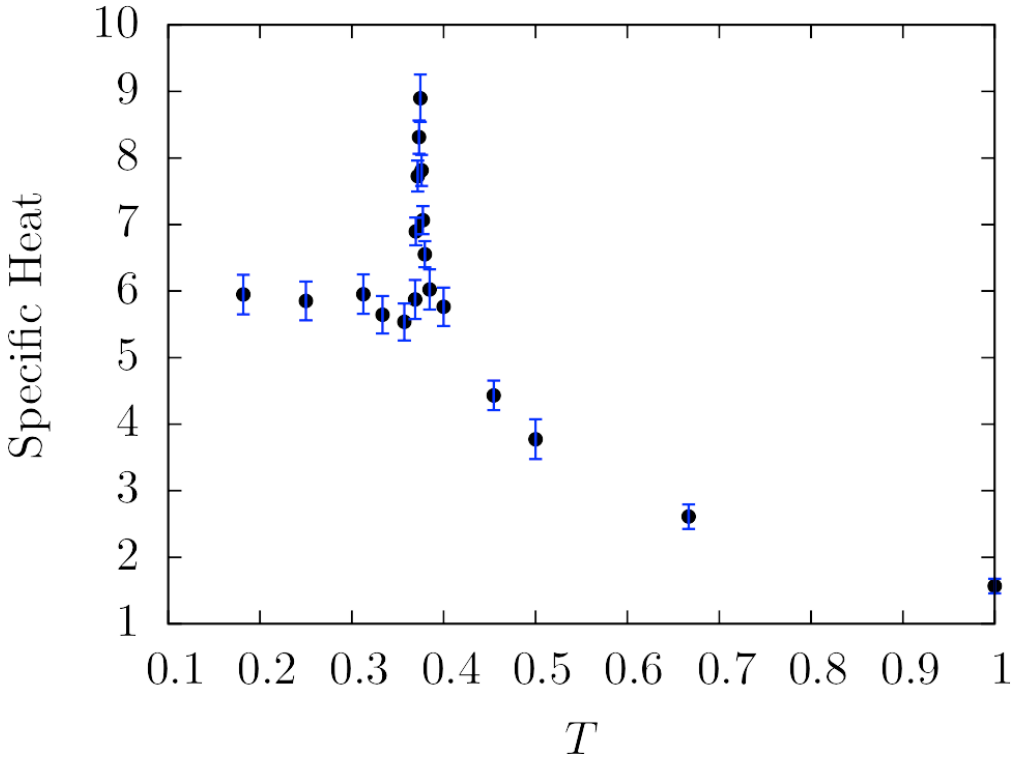

Figure 1.17: Specific heat for the cubic lattice SU(8) model with $N = 1000$ sites. The critical temperature is $T_c \simeq 0.370$.

the SU(8) singlet operator $\phi_\Gamma^\dagger$ on each cubic cell. Each site lies at the confluence of eight such cells, hence in the state $|\Psi\rangle = \prod_\Gamma (\phi_\Gamma^\dagger)^M |0\rangle$, each site is in the fully symmetric representation of SU(8) described by a Young tableau with one row and $8M$ boxes. Nearest neighbor cubes share a face, next nearest neighbor cubes share a single edge, and next next nearest neighbor cubes share a single site. The associated classical Hamiltonian for the model is constructed from eight-site interactions on every elementary cube of the lattice.

$$H_{cl} = -\sum_\Gamma \ln \left| \epsilon^{\alpha_1 \cdots \alpha_8} z_{\Gamma_1,\alpha_1} \cdots z_{\Gamma_8,\alpha_8} \right|^2 , \tag{1.27}$$

where Γ_i are the corners of the elementary cube Γ. A minimum energy ($E_0 = 0$) Potts state can be constructed by choosing eight mutually orthogonal vectors and arranging them in such a way that corners of every cube are different vectors from this set. Ground states of this model include all ground states of the eight-state Potts model with eight-spin interactions. Once again, a vast number of such Potts states is possible. For example, a state with alternating planes, each of them containing only four out of eight Potts spin directions, has a large number of zero modes. It has a simple cubic pattern, depicted in Fig. 1.16. We rely on numerical simulation to determine the preferred state at low temperatures.

There is a phase transition to the ordered phase at $T_c = 0.370 \pm 0.005$. This is backed by both heat capacity temperature dependence (Fig. 1.17) and static structure factor calculations. In the Fig. 1.18 the static structure factors for the SU(8) model on the cubic lattice are depicted. A and B are $k_z = 0$ and $k_z = \pi/a$ cross sections of the static factor in the ordered phase, $M = 20$. C and D are $k_z = 0$ and $k_z = \pi/a$ cross sections for higher temperature, $M = 2.7$, close to the critical value $M_C = 2.67 \pm 0.01$. E and F are $k_z = 0$ and $k_z = \pi/a$ cross

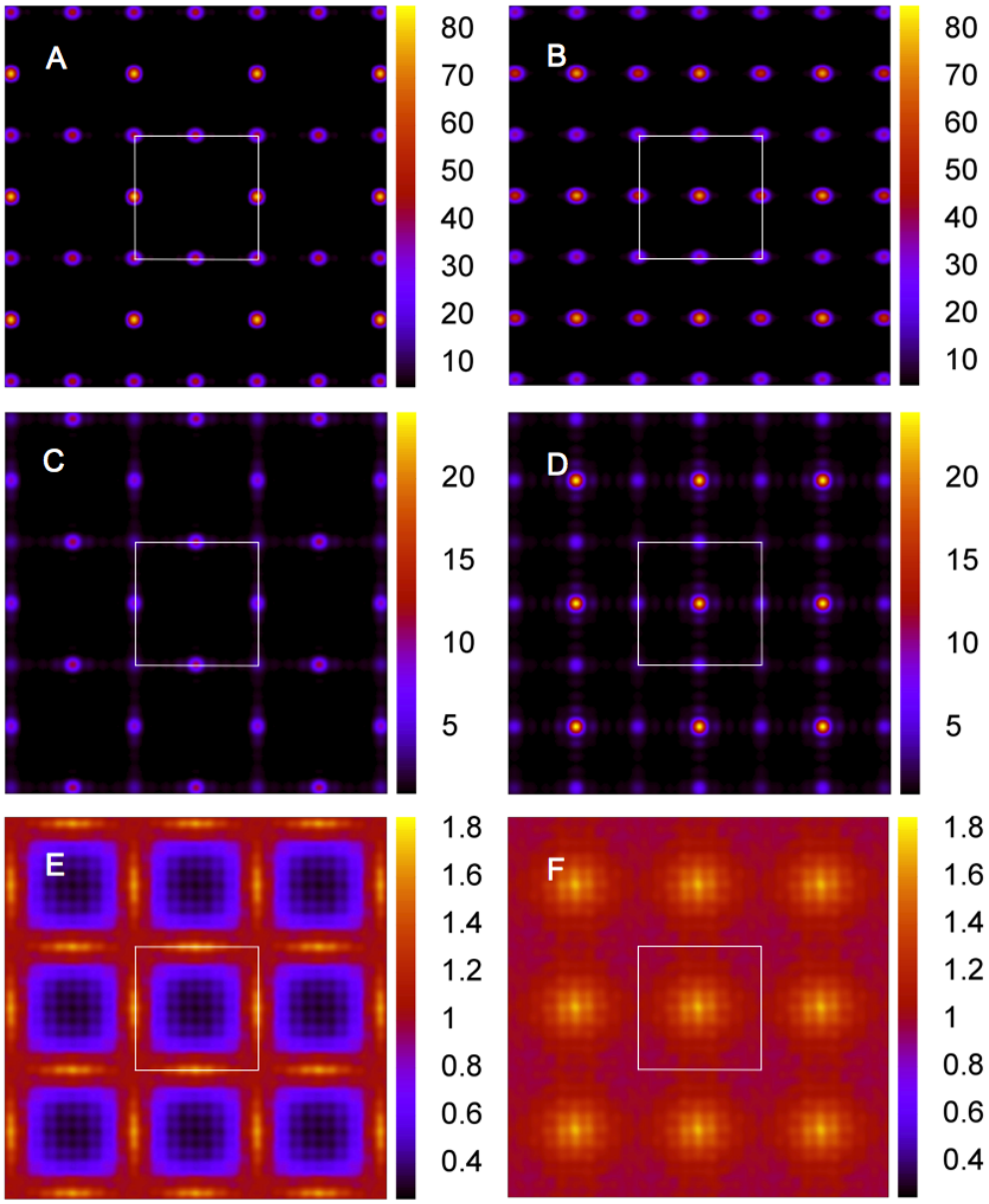

Figure 1.18: Static structure factors for the SU(8) model on the cubic lattice. Left panel A, C and E correspond to $k_z = 0$ cross sections of the static factor for $M = 20, 2.7$ and 2 respectively. Right panel B, D and F are $k_z = \pi/a$ respective cross sections.

sections in the disordered phase, $M = 2$. White lines denote the borders of the Brillouin zone. Number of sites is $N = 1000$. Note the overall scale – our Monte Carlo data for $S(\boldsymbol{k})$ indicates the presence of spontaneously broken SU(8) symmetry below T_c, where Bragg peaks develop corresponding to a simple cubic structure with a magnetic unit cell which is $2 \times 2 \times 2$ structural unit cells. Since $M_c = 1/T_c \simeq 2.70$, the SU(8) cubic lattice simplex solid states with $M = 1$ and $M = 2$ will be quantum disordered, while those with $M > 2$ will have 8-sublattice antiferromagnetic Potts order. As in the case of the SU(4) model discussed above, the actual transition temperature is larger than the mean field value $T_c^{\rm MF} = \zeta/(N^2 - 1) = \frac{8}{63} = 0.127$.

1.6.4 The mean field critical temperature

Conventional wisdom has it that mean field theory always overestimates the true T_c because of its neglect of fluctuations. As discussed in the introduction, in the SU(2) valence bond solid states, the corresponding classical interaction is $u_{ij} = -\ln\left(\frac{1}{2} - \frac{1}{2}\hat{\boldsymbol{n}}_i \cdot \hat{\boldsymbol{n}}_j\right)$, and one finds $T_c^{\rm MF} = r/3$, where r is the lattice coordination number. Monte Carlo simulations yield $T_c = 1.66$ on the cubic lattice ($r = 6$, $T_c^{\rm MF} = 2$), and $T_c = 0.85$ on the diamond lattice ($r = 4$, $T_c^{\rm MF} = \frac{4}{3}$) [5, 11]. In both cases, the mean field value $T_c^{\rm MF}$ overestimates the true transition temperature.

It is a simple matter, however, to concoct models for which the mean field transition temperature underestimates the actual critical temperature. Consider for example an Ising model with interaction $u(\sigma, \sigma') = -\epsilon^{-1} \ln(1 + \epsilon\sigma\sigma')$, where the spins take values $\sigma, \sigma' = \pm 1$, and where $0 < \epsilon < 1$. If we write $\sigma = \langle\sigma\rangle + \delta\sigma$ at each site and neglect terms quadratic in fluctuations, the resulting mean field Hamiltonian is equivalent to a set of decoupled spins in an external field $h = rm/(1 + \epsilon m^2)$. The mean field transition temperature is $T_c^{\rm MF} = r$, independent of ϵ.

On the other hand, we may also write $u(\sigma,\sigma') = u_\epsilon - J_\epsilon\,\sigma\sigma'$, where $u_\epsilon = -\ln(1-\epsilon^2)/2\epsilon$ and $J_\epsilon = \epsilon^{-1}\tanh^{-1}(\epsilon)$. On the square lattice, one has $T_c(\epsilon) = 2J_\epsilon/\sinh^{-1}(1)$, which diverges as $\epsilon \to 1$, while $T_c^{\rm MF} = 4$ remains finite. For $\epsilon > 0.9265$, one has $T_c(\epsilon) > T_c^{\rm MF}$.

Another example, suggested to us by S. Kivelson, is that of hedgehog suppression in the three-dimensional O(3) model. Motrunich and Vishwanath [34] investigated the O(3) model on a decorated cubic lattice with spins present at the vertices and at the midpoint of each link. They found $T_c = 0.588$ for the pure Heisenberg model and $T_c^* = 1.38$ when hedgehogs were suppressed. The mean field theory is not sensitive to hedgehog suppression, and one finds $T_c^{\rm MF} = \frac{2}{\sqrt{3}} = 1.15$, which overestimates T_c but underestimates T_c^*.

In both these examples, the mean field partition function includes states which are either forbidden in the actual model, or which come with a severe energy penalty ($\epsilon \approx 1$ in our first example). Consider now the classical interaction derived from the simplex-solid ground models, $u_\Gamma = -2\ln V_\Gamma$, where $V_\Gamma = |\epsilon^{\alpha_1\cdots\alpha_N} z_{\Gamma_1,\alpha_1}\cdots z_{\Gamma_N,\alpha_N}|$ is the internal volume of the simplex Γ. If we consider the instantaneous fluctuation of a single spin in the simplex, we see that there is an infinite energy penalty for it to lie parallel to any of the remaining $(N-1)$ spins, whereas the mean field Hamiltonian is of the form $H^{\rm MF} = -\zeta\sum_i h_{\mu\nu}(i)\,Q_{\mu\nu}(i)$, and $h_{\mu\nu}(i) = a_N(m)\delta_{\mu\nu} + b_N(m)\,P_{\mu\nu}^{\sigma(i)}$, where $a_N(m)$ and $b_N(m)$ are computed in Ref. [9], and $P^{\sigma(i)}$ is the projector onto the CP^2 vector associated with sublattice $\sigma(i)$ in a Potts ground state. There are no local directions which are forbidden by $H^{\rm MF}$, so the mean field Hamiltonian allows certain fluctuations which are forbidden by the true Hamiltonian. This state of affairs also holds for the SU(2) models, where Monte Carlo simulations found that the mean field transition temperature overestimates the true transition temperature, as the folk theorem says, but

apparently the difference $T_c - T_c^{MF}$ becomes positive for larger values of N.

1.7 Order and Disorder in Simplex Solid States

To apprehend the reason why the SU(3) hyperkagome model remains disordered for all $T = 1/M$ while the SU(4) and SU(8) cubic lattice models have finite T phase transitions (which in the former case lies in the forbidden regime $T > 1$, *i.e.* $M < 1$), we examine once again the effective low-temperature Hamiltonian of eqn. 1.9, derived in Ref. [9],

$$H_{\rm LT} = \sum_{\Gamma} \sum_{i<j}^{N} \left| \pi^\dagger_{\Gamma_i} \, \omega_{\sigma(\Gamma_j)} + \omega^\dagger_{\sigma(\Gamma_i)} \pi_{\Gamma_j} \right|^2 \quad . \tag{1.28}$$

The expansion here is about a Potts state, where each simplex Γ is fully satisfied such that $V_\Gamma = 1$. In a Potts state, each lattice site k is assigned to a sublattice $\sigma(k) \in \{1, \ldots, N\}$, with $\{\omega_\sigma\}$ a mutually orthogonal set of N CP^{N-1} vectors and $\pi_i^\dagger \omega_{\sigma(i)} = 0$. It is convenient to take $\omega_{\sigma,\mu} = \delta_{\mu,\sigma}$, *i.e.* the μ component of the CP^{N-1} vector ω_σ is $\delta_{\mu,\sigma}$. In $H_{\rm LT}$, the first sum is over all simplices Γ, and the second sum is over all pairs of sites (Γ_i, Γ_j) on the simplex Γ.

Let us first consider a Potts state which has the same periodicity as the underlying lattice. In such a state, each simplex corresponds to a unit cell of the lattice. Examples would include the $\boldsymbol{q} = 0$ Potts states of the SU(3) simplex solid on the kagome lattice and the SU(4) model on the pyrochlore lattice, or a variant of the SU(8) cubic lattice model discussed above, where one sublattice of cubes is eliminated such that the remaining cubes are all corner-sharing. In such a structure, we may write $\omega_{\sigma(\Gamma_i)} \equiv \omega_i$, in which case the interaction between sites i and j on the same simplex may be written as $|\pi^*_{\Gamma_i, j} + \pi_{\Gamma_j, i}|^2$, where $\pi_{\Gamma_i, j}$

is the j component of the N-component vector π_{Γ_i}. Note that $\pi_{\Gamma_i,i} = 0$. Since each site is a member of precisely two simplices, the system may be decomposed into a set of one-dimensional chains, each of which is associated with a pair (σ,σ') of indices. Hence there are $\frac{1}{2}N(N-1)$ pairs in all. To visualize this state of affairs, it is helpful to refer to the case of the kagome lattice in fig. 1.2, for which $N = \frac{1}{2}N(N-1) = 3$. Thus there are three types of chains: AB, BC, and CA. Each AB chain is described by a classical energy function of the form

$$\begin{aligned} H_{\rm AB} &= \sum_n \Big(|a_n^* + b_n|^2 + |b_n^* + a_{n+1}|^2 \Big) \\ &= \sum_k \begin{pmatrix} a_k^* & b_{-k} \end{pmatrix} \begin{pmatrix} 2 & 1+e^{-ik} \\ 1+e^{ik} & 2 \end{pmatrix} \begin{pmatrix} a_k \\ b_{-k}^* \end{pmatrix} \quad . \end{aligned} \tag{1.29}$$

This yields two excitation branches, with dispersions $\omega_\pm(k) = 2 \pm 2\cos(\frac{1}{2}k)$. Thus we recover $N(N-1)$ complex degrees of freedom, or $2N(N-1)$ real degrees of freedom, per unit cell, as derived in §1.3.1.

In Ref. [9], the fixed length constraint of each CP^{N-1} vector z_i was approximated by implementing the nonholonomic constraint $\langle \pi_i^\dagger \pi_i \rangle \le 1$, which in turn is expressed as $|\chi|^2 + \langle \pi_i^\dagger \pi_i \rangle = 1$, where χ plays the role of a condensate amplitude. This holonomic constraint is enforced with a Lagrange multiplier λ, so that the free energy per site takes the form of eqn. 1.18, where $g(\varepsilon)$ is the total density of states per site, normalized such that $\int_0^\infty d\varepsilon\, g(\varepsilon) = 1$. For the models

currently under discussion, we have $g(\varepsilon) = g_{1D}(\varepsilon)$, where

$$\begin{aligned} g_{1D}(\varepsilon) &= \int_0^{2\pi} \frac{d\theta}{2\pi}\, \delta(2 - 2\cos\theta - \varepsilon) \\ &= \frac{\Theta\Big(2 - |\varepsilon - 2|\Big)}{\pi\sqrt{\varepsilon(4-\varepsilon)}} \quad , \end{aligned} \tag{1.30}$$

characteristic of one-dimensional hopping. The spectrum is confined to the interval $\varepsilon \in [0, 4]$, and extremizing with respect to λ yields the equation

$$1 = |\chi|^2 + (N-1)\, T \int_0^\infty d\varepsilon\, \frac{g(\varepsilon)}{\varepsilon + \lambda} \quad . \tag{1.31}$$

If $\int_0^\infty d\varepsilon\, \varepsilon^{-1} g(\varepsilon) < \infty$, then $\lambda = 0$ and $|\chi|^2 > 0$. This is the broken SU(N) symmetry regime. Else, $\lambda > 0$ and $\chi = 0$, corresponding to a gapped, quantum disordered state.

1.7.1 SU(3) kagome and hyperkagome models

For the SU(3) kagome and hyperkagome models, expanding about a $\boldsymbol{q} = 0$ Potts state, the free energy per site for the low temperature model $H_{\rm LT}$, implementing the nonholonomic mean fixed length constraint for the CP^2 spins, is found to be

$$f(T, \lambda) = -\lambda + 2T \ln\left(\frac{2 + \lambda + \sqrt{\lambda(\lambda+4)}}{2T} \right) \quad . \tag{1.32}$$

Setting $\partial f/\partial\lambda = 0$ yields $\lambda = 2\Big(\sqrt{1+T^2} - 1\Big)$. These systems are in gapped, disordered phases for all T, meaning that the corresponding quantum wave functions are quantum-disordered for all values of the discrete parameter M. The low temperature specific heat is $C(T) = 2 - 2T + \mathcal{O}(T^2)$.

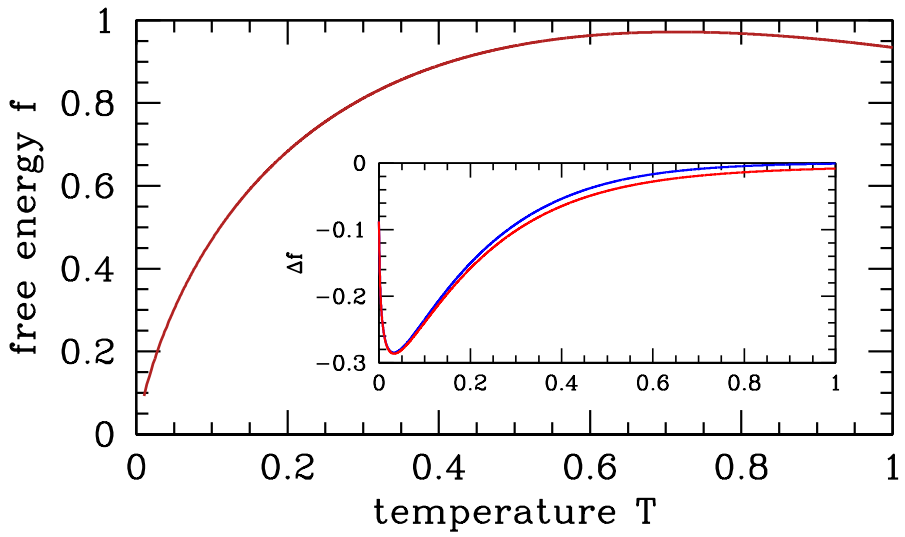

Figure 1.19: Free energy per site for the $\boldsymbol{q} = 0$ states of the SU(3) kagome and hyperkagome lattice models. The inset shows the difference in free energies Δf between the $\sqrt{3} \times \sqrt{3}$ and $\boldsymbol{q} = 0$ structures for the kagome and the hyperkagome lattices.

Free energy per site for the $\boldsymbol{q} = 0$ states of the SU(3) kagome and hyperkagome lattice models. The inset shows the difference in free energies Δf between the $\sqrt{3} \times \sqrt{3}$ structure on the kagome lattice and the $\boldsymbol{q} = 0$ state (blue), and the corresponding difference for the analogous state in the hyperkagome lattice (36 site magnetic unit cell).

In the $\sqrt{3} \times \sqrt{3}$ state on the kagome lattice, we have [9]

$$g_{\mathrm{K}}(\varepsilon) = \tfrac{1}{6}\Big\{\delta(\varepsilon) + 2\,\delta(\varepsilon - 1) + 2\,\delta(\varepsilon - 3) + \delta(\varepsilon - 4)\Big\}\,, \tag{1.33}$$

whereas for the analogous structure in the hyperkagome lattice, with a 36 site

magnetic unit cell, we find

$$g_{\rm HK}(\varepsilon) = \tfrac{1}{12}\Big\{2\,\delta(\varepsilon) + \delta(\varepsilon-1) + 2\,\delta(\varepsilon-2) + \delta(\varepsilon-3) \\ + 2\,\delta(\varepsilon-4) + \delta(\varepsilon-1-\phi) + \delta(\varepsilon-2+\phi) \\ + \delta(\varepsilon-2-\phi) + \delta(\varepsilon-3+\phi)\Big\} \quad , \tag{1.34}$$

where $\phi = \frac{1}{2}\left(1+\sqrt{5}\right) \simeq 1.618$. For the kagome system, we obtain

$$\frac{1}{T} = \frac{2u}{3}\cdot\left\{\frac{1}{u^2-4} + \frac{2}{u^2-1}\right\} \quad , \tag{1.35}$$

where $u \equiv \lambda + 2$. For the hyperkagome system,

$$\frac{1}{T} = \frac{u}{3}\cdot\left\{\frac{2}{u^2-4} + \frac{1}{u^2-\phi^2} \right. \\ \left. + \frac{1}{u^2-1} + \frac{1}{u^2-(1-\phi)^2} + \frac{1}{u^2}\right\}. \tag{1.36}$$

One then obtains $\lambda_{\rm K} = \frac{1}{3}T + \frac{35}{108}T^2 + \mathcal{O}(T^3)$ for kagome $\lambda_{\rm HK} = \frac{1}{3}T + \frac{31}{108}T^2 + \mathcal{O}(T^3)$ for hyperkagome, at low temperatures. The corresponding specific heat functions are then

$$C_{\rm K}(T) = \tfrac{5}{3} - \tfrac{35}{54}\,T + \mathcal{O}(T^2) \\ C_{\rm HK}(T) = \tfrac{5}{3} - \tfrac{31}{54}\,T + \mathcal{O}(T^2)\,. \tag{1.37}$$

Both tend to the same value as $T \to 0$. For the kagome system, we found $C(0) = 1.84 \pm 0.03$, close to the value of $\frac{16}{9}$ obtained by augmenting the quadratic mode contribution of $\frac{5}{3}$ with that from the quartic modes, whose contribution is $\Delta C = \frac{1}{9}$. Our hyperkagome simulations, however, found $C(0) \approx 2$, with no apparent deficit from zero modes or quartic modes. Again, this is consistent

with the structure factor results, which show no hint of any discernible structure down to the lowest temperatures. A plot of the free energy per site for the $\boldsymbol{q} = 0$ Potts state on the kagome and hyperkagome lattices, and the free energy difference per site between this structure and the $\sqrt{3} \times \sqrt{3}$ kagome structure and its hyperkagome analog are shown in Fig. 1.19. The inset of the figure shows the difference in free energies Δf between the $\sqrt{3} \times \sqrt{3}$ structure on the kagome lattice and the $\boldsymbol{q} = 0$ state (blue), and the corresponding difference for the analogous state in the hyperkagome lattice, which magnetic unit cell consists of 36 sites.

1.7.2 SU(4) cubic lattice model

We now analyze the low-energy effective theory of the SU(4) cubic lattice model, expanding about the Potts state depicted in fig. 1.12. The magnetic unit cell consists of four sites. Let the structural cubic lattice constant be $a \equiv 1$. The magnetic Bravais lattice is then BCC, with elementary direct lattice vectors

$$\boldsymbol{a}_1 = (1,1,1) \quad , \quad \boldsymbol{a}_2 = (-1,1,1) \quad , \quad \boldsymbol{a}_3 = (1,-1,1)$$

and elementary reciprocal lattice vectors

$$\boldsymbol{b}_1 = (\pi,\pi,0) \quad , \quad \boldsymbol{b}_2 = (-\pi,0,\pi) \quad , \quad \boldsymbol{b}_3 = (0,-\pi,\pi)\,.$$

In the Potts state, the A sites lie at BCC Bravais lattice sites $\boldsymbol{R}$, with B sites at $\boldsymbol{R}+\hat{\boldsymbol{x}}$, C at $\boldsymbol{R}+\hat{\boldsymbol{y}}$, and D at $\boldsymbol{R}+\hat{\boldsymbol{z}}$. There are $2(N-1) = 6$ real degrees of freedom per lattice site, and hence 24 per magnetic unit cell. The low temperature Hamiltonian may

be written as a sum of six terms

$$H_{\rm LT} = H_{\rm AB} + H_{\rm AC} + H_{\rm AD} + H_{\rm BC} + H_{\rm BD} + H_{\rm CD} \quad , \tag{1.38}$$

where $H_{\rm AB}$ couples the B component of the π vector on the A sites with the A component of the π vector on the B sites. Explicitly, we note that an A site at $\boldsymbol{R}$ has B neighbors in unit cells at $\boldsymbol{R}$, at $\boldsymbol{R}-\boldsymbol{a}_1$, at $\boldsymbol{R}+\boldsymbol{a}_2$, at $\boldsymbol{R}-\boldsymbol{a}_3$, at $\boldsymbol{R}-\boldsymbol{a}_1+\boldsymbol{a}_2$, and at $\boldsymbol{R}-\boldsymbol{a}_1+\boldsymbol{a}_2+\boldsymbol{a}_3$. Thus,

$$\begin{aligned} H_{\rm AB} &= \sum_{\boldsymbol{R}} \Big\{ b^*_{\boldsymbol{R}} \Big(a_{\boldsymbol{R}} + a_{\boldsymbol{R}-\boldsymbol{a}_1} + a_{\boldsymbol{R}+\boldsymbol{a}_2} + a_{\boldsymbol{R}-\boldsymbol{a}_3} + a_{\boldsymbol{R}-\boldsymbol{a}_1+\boldsymbol{a}_2} \\ &\qquad + a_{\boldsymbol{R}-\boldsymbol{a}_1+\boldsymbol{a}_2+\boldsymbol{a}_3} \Big) + \text{c.c.} + 6|a_{\boldsymbol{R}}|^2 + 6|b_{\boldsymbol{R}}|^2 \Big\} \\ &= 6 \sum_{\boldsymbol{k}} \begin{pmatrix} a^*_{\boldsymbol{k}} & b_{-\boldsymbol{k}} \end{pmatrix} \begin{pmatrix} 1 & \gamma_{\boldsymbol{k}} \\ \gamma^*_{\boldsymbol{k}} & 1 \end{pmatrix} \begin{pmatrix} a_{\boldsymbol{k}} \\ b^*_{-\boldsymbol{k}} \end{pmatrix} \quad , \end{aligned} \tag{1.39}$$

where

$$\begin{aligned} \gamma_{\boldsymbol{k}} = \tfrac{1}{3} e^{i(\theta_2-\theta_1)/2} \Big\{ &\cos\left(\frac{\theta_1-\theta_2}{2}\right) + \cos\left(\frac{\theta_1+\theta_2}{2}\right) \\ &+ \cos\left(\frac{\theta_1-\theta_2}{2} - \theta_3\right) \Big\} \end{aligned} \tag{1.40}$$

with $\boldsymbol{k} = \frac{1}{2\pi} \sum_{i=1}^{3} \theta_i \boldsymbol{b}_i$. This leads to two bands, with dispersions $\omega_{\pm}(\boldsymbol{k}) = 6\big(1 \pm |\gamma_{\boldsymbol{k}}|\big)$. All the other Hamiltonians on the RHS of eqn. 1.38 yield the same dispersion. Counting degrees of freedom, we have four real (two complex) modes per $\boldsymbol{k}$ value ($\mathrm{Re}\, a_{\boldsymbol{k}}$, $\mathrm{Im}\, a_{\boldsymbol{k}}$, $\mathrm{Im}\, b_{\boldsymbol{k}}$ and $\mathrm{Im}\, b_{\boldsymbol{k}}$), and six independent Hamiltonians on in eqn. 1.38, corresponding to 24 real modes per unit cell, as we found earlier. The bottom of the $\omega_-(\boldsymbol{k})$ band lies at $|\gamma_{\boldsymbol{k}}| = 1$, which entails $\theta_1 = \theta_2 = \theta_3 = 0$. Expanding about this point, the dispersion is quadratic in deviations, corre-

sponding to the familiar bottom of a parabolic band. The density of states is then $g(\varepsilon) \propto \sqrt{\varepsilon}$, which means that $\lambda = 0$ and $|\chi(T)|^2$ interpolates between $|\chi(0)|^2 = 1$ and $|\chi(T_c)|^2 = 0$, where

$$T_c = \frac{1}{(N-1)\int_0^\infty d\varepsilon\, \varepsilon^{-1} g(\varepsilon)} \tag{1.41}$$

is the prediction of the low energy effective theory. Because the low-temperature effective hopping theory for edge-sharing (and face-sharing) simplex solids involves fully three-dimensional hopping, the band structure of their low-lying excitations features parabolic minima, which in turn permits a solution with $\lambda \neq 0$, meaning the ordered state is stable over a range of low temperatures. We find $T_c = 1.978$ for the edge-sharing simplex solid model on the simple cubic lattice. This is substantially greater than both the mean field result $T_c^{\mathrm{MF}} = \frac{4}{5}$ and the Monte Carlo result $T_c \simeq 1.485$.

1.8 Conclusions

We have studied the structure of exact simplex solid ground states of SU(N) spin models, in two and three dimensions, via their corresponding classical companion models that encode their equal time correlations. The discrete parameter M which determines the on-site representation of SU(N) sets the temperature $T = 1/M$ of each classical model, which then may be studied using standard tools of classical statistical mechanics. Our primary tool is Monte Carlo simulation, augmented by results from mean field and low-temperature effective theories. This work represents an extension of earlier work on SU(2) AKLT models.

Through a study of representative models with site-, edge-, and face-

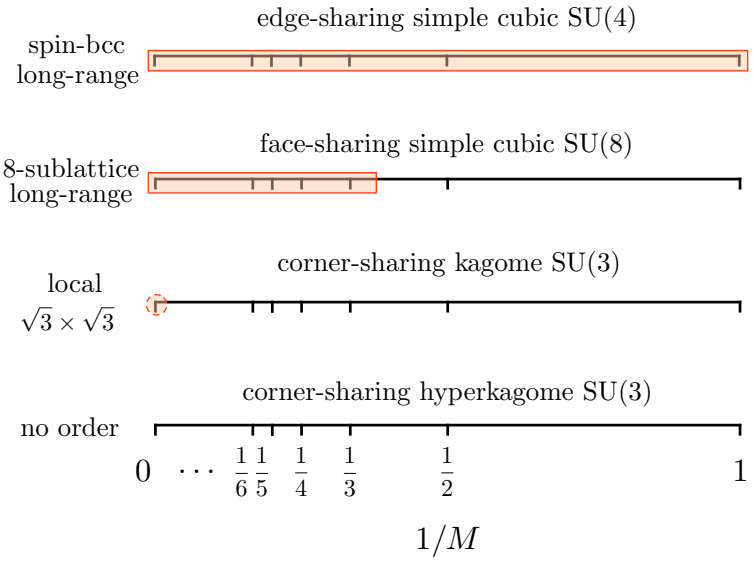

Figure 1.20: Structure of simplex solids as a function of discrete parameter M. The parameter range for which long-range (local) order emerges is shaded and bounded by solid (dashed) lines.

sharing simplices, we identify three broad categories of simplex solids, based on the T-dependence of the associated classical model:

1. Models which exhibit a phase transition in which SU(N) is broken at low temperature, corresponding to a classical limit $M \to \infty$ analogous to $S \to \infty$ for SU(2) systems, as exemplified by the edge-sharing SU(4) and face-sharing SU(8) cubic lattice simplex solids. Whether or not these models have quantum-disordered for physical (i.e., integer) values of the singlet parameter M depends on the precise value of the transition temperature.

2. Models which exhibit no phase transition down to $T = 0$, but reflect strong local ordering which breaks lattice and SU(N) symmetries, as in the SU(3) model on the kagome lattice. While the low and high M limits of these simplex solids appear to be in the same (quantum-disordered) phase, we expect the ground state expectation values for $M \to \infty$ are dominated by

classical configurations with a large density of local zero modes.

3. Models which exhibit neither a phase transition nor apparent local order down to $T = 0$ and are hence quantum-disordered and featureless for all M. These simplex solids perhaps best realize the original AKLT ideal of a featureless quantum-disordered paramagnet, for the case of SU(N) spins. The hyperkagome lattice SU(3) simplex solid is representative of this class.

These results are summarized graphically in Fig. 1.20. Whereas on the cubic lattice the edge-sharing SU(4) model is always long-ranged ordered, the face-sharing SU(8) model has quantum-disordered ground states for $M = 1, 2$. The SU(3) model exhibits quantum disorder for all M, with local $\sqrt{3}\times\sqrt{3}$ correlations strengthening as $M \to \infty$ on the kagome lattice while on the hyperkagome, no local or long range order is apparent at any M.

The parent Hamiltonians which admit exact simplex solid ground states are baroque and bear little resemblance to the simple SU(N) Heisenberg limit typically studied. Nevertheless, we may regard the simplex solids as describing a phase of matter which may include physically relevant models. This state of affairs obtains in $d = 1$, where the AKLT state captures the essential physics of the $S = 1$ Heisenberg antiferromagnet in the Haldane phase. We also note that SU(N) magnetism, once primarily a theorists' toy, may be relevant in certain experimental settings; in this context, there has been recent progress examining the feasibility of realizing such generalized spin models with systems of ultracold atoms, particularly those involving alkaline earth atoms [35, 36]. Whether the states analyzed in this chapter will find a place in the phase diagrams of such systems remains an open question, that we defer to the future.

Chapters 1 contains material from the paper:

Y.Y. Kiselev, S.A. Parameswaran, and D.P. Arovas, "Order and disorder in SU(N) simplex solid antiferromagnets", *Journal of Statistical Mechanics: Theory and Experiment*, 013105, (2016). The dissertation author was the primary investigator and author of this paper.

Chapter 2

Quantum critical behavior of the superfluid-Mott transition

One of the examples of quantum phase transitions is a zero-temperature phase transition between superfluid and insulating ground states in a system of disordered interacting bosons. Depending on the parameters of the system, the phases of Mott insulator and superfluid are separated by another phase, the Bose glass phase [37]. We are studying the critical properties of the superfluid-Mott glass quantum phase transition and the model under consideration is a diluted quantum rotor in two spatial dimensions.

2.1 Introduction

Hubbard model describes transition between insulating and conducting states occurring in the systems of interacting bosons on the lattice. Its Hamiltonian

$$H = -t \sum_{\langle i,j \rangle} (b_i^\dagger b_j + b_j^\dagger b_i) + \frac{U}{2} \sum_i \hat{n}_i(\hat{n}_i - 1) - \mu \sum_i \hat{n}_i, \tag{2.1}$$

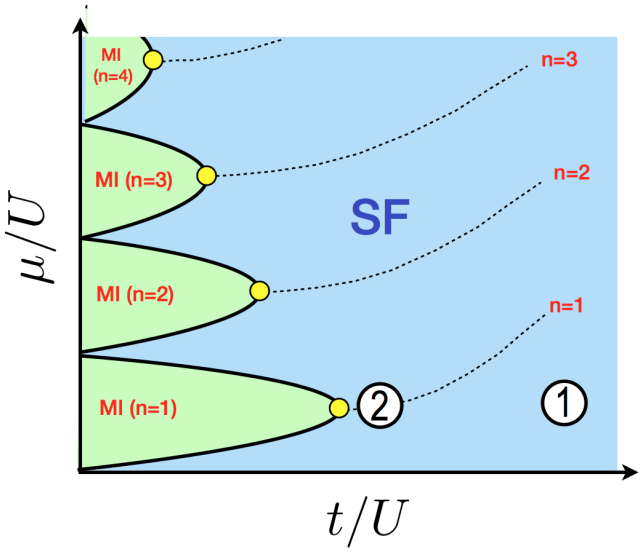

Figure 2.1: Phase diagram of the Hubbard model. Mott lobes are depicted as yellow dots, and region (2) are the points close to one of the Mott lobes.

and for small t/U the system is a Mott insulator, while for large t/U the system is a superfluid. The phase diagram is plotted on the Fig. 2.1 and shows two qualitatively different regions of the superfluid phase: (1) are the points far from Mott lobes, where the system is described by Gross-Pitaevski model

$$\mathcal{L}_1 = -i\psi^*\partial_t\psi - \frac{\hbar^2}{2m^*}|\nabla\psi|^2 + \mu|\psi|^2 - g|\psi|^4. \tag{2.2}$$

This description has a gapless Goldstone mode, but no Higgs (amplitude) mode.

Region (2) corresponds to the points close to the Mott lobes, where the system is described by the relativistic $|\psi|^4$-model,

$$\mathcal{L}_2 = |\partial_t\psi|^2 - c^2|\nabla\psi|^2 + r|\psi|^2 - u|\psi|^4. \tag{2.3}$$

In the second case both Goldstone and Higgs (amplitude) modes are present.

While we are interested in the phase diagram of the 2D diluted $|\psi|^4$-model. The fate of the clean $|\psi|^4$-model was researched by Gazit et al. in [38], where

they studied the model

$$\mathcal{Z} = \int \mathcal{D}\vec{\phi} e^{-S[\vec{\phi}]}$$
$$S = \sum_{\langle i,j \rangle} \vec{\phi}_i \cdot \vec{\phi}_j + \mu \sum_i |\vec{\phi}_i|^2 + g \sum_i |\vec{\phi}_i|^4, \tag{2.4}$$

and found that for two-dimensional system there are two phases, one with Higgs mode in ordered phase for low $g < g_c$, and the disordered one for $g > g_c$.

2.2 The model

The field theory in Euclidian space-time $(2+1)$ dimensions is

$$\mathcal{Z} = \int \mathcal{D}\vec{\phi} e^{-S[\vec{\phi}]}$$
$$S[\vec{\phi}] = \int \mathrm{d}x\mathrm{d}\tau \{-\tfrac{1}{2}(\partial_q \vec{\phi})^2 - \tfrac{1}{2}\mu|\vec{\phi}_i|^2 + g|\vec{\phi}_i|^4\}, \tag{2.5}$$

where the fields are N-component fields and index $q = \{x, y, \tau\}$. Such field theory describes a transition of superfluid to Mott insulator at commensurate fillings for $N = 2$ [39], and for $N = 3$ example is the Néel to singlet transition for the dimerized Heisenberg antiferromagnets [40].

We make the field theory 2.5 more realistic and interesting by considering the discrete lattice model with dilution. Dilution eliminates some sites in the original two-dimensional model and thus creates columnar disorder in our classical (2+1)-dimensional model, see Fig. 2.2. We will study $N = 2$ case, which

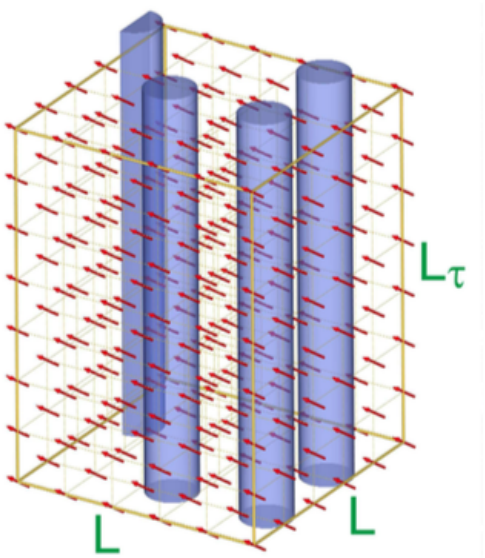

Figure 2.2: Sketch of the $(2+1)$-dimensional lattice with the dilution (pink columns).

is equivalent to the complex $|\phi|^4$-model.

$$\mathcal{Z} = \int \mathcal{D}\phi\mathcal{D}\phi^* e^{-S[\phi,\phi^*]}$$
$$S = -\frac{1}{2}\sum_{\langle i,j\rangle}(\phi_i\phi_j^* + \phi_i^*\phi_j) - \mu\sum_i |\phi_i|^2 + g\sum_i |\phi_i|^4. \tag{2.6}$$

Here the complex field ϕ_i is residing on the remaining after dilution sites of the $(2+1)$-dimensional lattice. The spatial size is L in x and y direction, and the temporal length of the lattice is $L_\tau = L^z$, where z is the critical exponent to be found later.

2.3 Worm algorithm

Worm algorithm is a Monte Carlo-type numerical algorithm that represents terms of the high-temperature expansion of the partition function as the configurations of closed loops. Then Markov chain procedure is used to sample

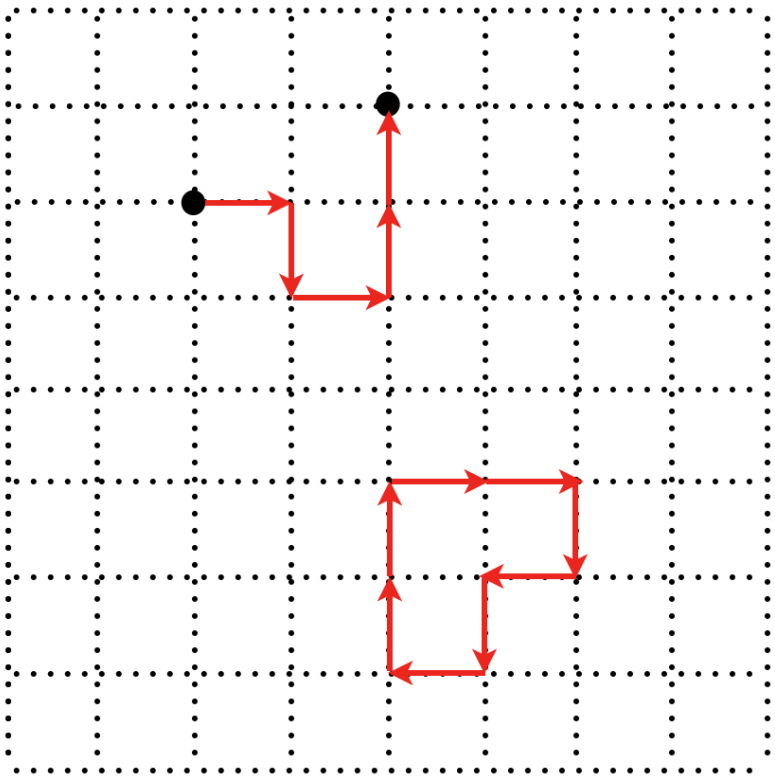

Figure 2.3: Example of worms. Closed loops only configurations yield non-zero contributions for the partition function. Open configuration yield non-zero contributions to the correlation function $G(i,j) = \langle \phi_i \phi_j^* \rangle$.

the terms of the expansion with the detailed balance probabilities proportional to their corresponding weights in the partition function expression.

For the model 2.4 we need to expand the expression in terms of contributions of the pairs $\phi_i \phi_j$, where i, j are the nearest neighbors. We are proceeding in the similar way as Gazit et al. in [38]. We are studying O(2) model with complex field ϕ, so that

$$\mathcal{Z} = \int \mathcal{D}\phi \mathcal{D}\phi^* e^{-S[\phi,\phi^*]}$$
$$S = -\tfrac{1}{2} \sum_{\langle i,j \rangle} (\phi_i \phi_j^* + \phi_i^* \phi_j) - \mu \sum_i |\phi_i|^2 + g \sum_i |\phi_i|^4. \tag{2.7}$$

First let's expand partition function in the nearest-neighbor coupling:

$$\mathcal{Z} = \int \mathcal{D}\phi\mathcal{D}\phi^* \prod_b \sum_{n_b} \frac{1}{2^{n_b} n_b!} (\phi^*_{i_b} \phi_{i'_b})^{n_b} \prod_j e^{(\mu|\phi_j|^2 - g|\phi_j|^4)} \tag{2.8}$$

Here each term $\phi^*_{i_b}\phi_{i'_b}$ can be depicted on the lattice as a directed link from site i_b to the site i'_b, b is the directional link between two neighboring sites, and the total amount of the oriented links from the site i_b to the site i'_b in the given direction is specified by n_b. The expression above corresponds to the sum of configurations of the directed links with the weights dictated by the integral, taking into account as well the onsite interaction $\prod_j e^{(-\mu|\phi_j|^2 - g|\phi_j|^4)}$. Let's note that the configuration of the lattice bonds will yield zero after integration if it's not a combination of directed closed loops. Indeed, integrals like the one below are non-zero,

$$\int \mathcal{D}\phi\mathcal{D}\phi^* \prod_c (\phi^*_{i_c} \phi_{i'_c})^{n_c} e^{-V(|\phi|)} \neq 0 \tag{2.9}$$

if each field ϕ^*_i enters the integral the same number of times as ϕ_i for each site i. If we represent each term $\phi^*_i \phi_{i'}$ as a directed link from site i to i', only configurations that consist of superposition of closed loops (see Fig. 2.3) on the lattice will yield non-zero contributions. We can find the non-zero contributions by integrating field ϕ_i. The partition function becomes a product of single-site integrals:

$$\mathcal{Z} = \sum_{\{n_b\}} \prod_b \frac{1}{2^{n_b} n_b!} \prod_i W(k_i), \tag{2.10}$$

where $k_i = \sum_{b(i)} n_b$ is the number of all the links going out of site i, which equals

to the number of the links going into the site i. So the single-site weight is

$$W(k_i) = \int \mathrm{d}\phi_i \mathrm{d}\phi_i^* \, |\phi_i|^{2k_i} e^{(\mu|\phi_i|^2 - g|\phi_i|^4)} = \pi \int_0^\infty \mathrm{d}s \; s^{k_i} e^{(\mu s - g s^2)}. \tag{2.11}$$

This integral can be tabulated prior to the numerical simulation.

The Worm Algorithm procedure that yields terms of the high-T expansion with appropriate weights is based on the following idea [4]. Each loop corresponds to a term in the partition function, but it's problematic to make local updates to the loop structure that will switch from one loop to another with desired detailed balance probability. Instead, let's enlarge the configuration space of the loops, by including also configurations of the links that have only one open loop and any number of closed loops. Such configurations correspond to the correlation function $G(I,M) = \langle \phi_I^* \phi_M \rangle$. We will make local updates in the enlarged space of the configurations by removing or adding the link to the existing configuration. Only when sites I and M coincide, the configuration consists only of closed loops, and contributes to the calculation of partition function. All updates to the bond configuration are made on the end-points of the open configuration. There are two types of moves

1. *Shift move*. During this move we either add a link to the worm's head, or erase the existing link that ends at the worm's head. So the worm's head moves correspondingly to a neighboring site.

2. *Jump move*. This move is relevant only for the closed-loop configuration when the ends of the worm coincide: $I = M$. During this move we can reassign position of both ends to any other site of the lattice.

The acceptance ratios of the moves can be calculated from the equation 2.11:

$$\begin{aligned} P_{shift}(i \to j, n_b \to n_b + 1) &= \frac{1}{2(n_b+1)} \frac{W(k_j+1)}{W(k_j)}, \\ P_{shift}(i \to j, n_b \to n_b - 1) &= 2n_b \frac{W(k_i-1)}{W(k_i)}, \\ P_{jump}(i \to j) &= \frac{W(k_j+1)}{W(k_j)} \frac{W(k_i-1)}{W(k_i)}. \end{aligned} \tag{2.12}$$

After this the Monte Carlo estimator for $\mathcal{Z}$ is just

$$\mathcal{Z}(\{n_b\}) = \delta_{I,M}. \tag{2.13}$$

Then the algorithm is the following:

- Start with $I = M$ assigned to some random lattice site.
- For every turn: if the configuration consists only from closed loops, perform the jump move with the given probability.
- For every turn: choose with probability 1/2 whether to add or erase bonds, choose randomly a direction, and either change bond configuration or not given by P_{shift}.

It was shown by [4] that Worm algorithm doesn't have critical slowing down close to the critical point, so it fits well to explore critical properties of the problem.

2.4 Results

Our collaborators performed a Monte Carlo simulations using conventional Metropolis updates and Wolff cluster algorithm. Their large-scale simulation determined the phase diagram of the hard-spin system for different

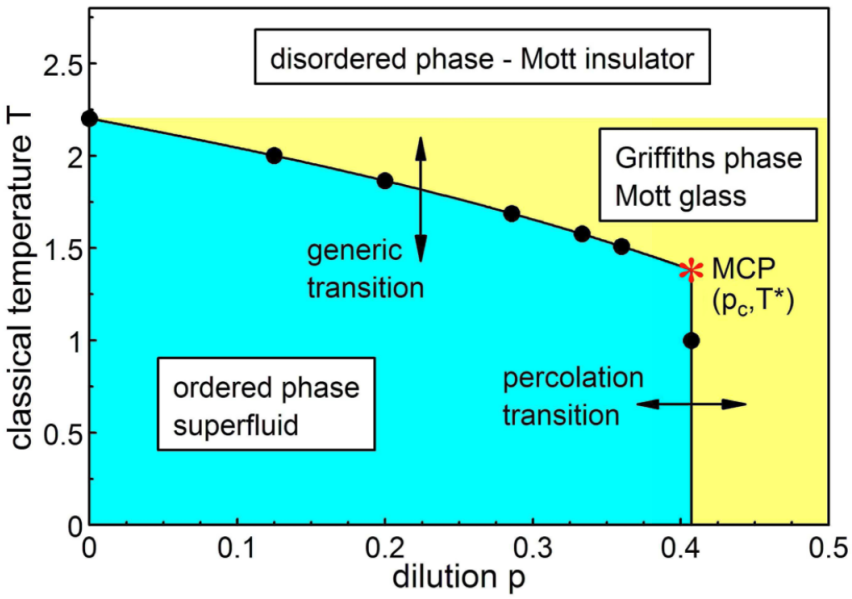

Figure 2.4: Phase diagram of the classical XY model as a function of classical temperature and dilution. The big dots mark the numerically determined transition points. The lines are guides for the eye only..

levels (percentages) of dilution p and classical temperature T, see Fig. 2.4. They determined a critical exponent $z = 1.52(3)$ and $\nu = 1.16(5)$.

For a given dilution level, we can determine location of the critical coupling g_c by the finite-size scaling analysis of the helicity modulus of our $(2+1)$-dimensional model. The helicity modulus $\Upsilon = \frac{1}{L}\frac{\partial^2 \ln \mathcal{Z}(\varphi)}{\partial^2 \varphi^2}|_{\varphi=0}$, where we introduced uniform phase twist φ to the system. Close to the critical point $\rho_s = \Upsilon L$ is universal constant, which allows to determine g_c from the crossing point of $\rho_s = L\Upsilon$. We find the helicity modulus from the winding statistics of the directed worms on the lattice: $\rho_s = \langle W^2 \rangle$, where W is a winding number, i.e. a number of times the worm wraps around the lattice.

Our own computing power was not sufficient to find the dynamical critical exponent z, but our collaborators [41] obtained $z \approx 1.5$, which we used to obtain data collapse for the correlation length ξ_τ. We performed simulations, studying

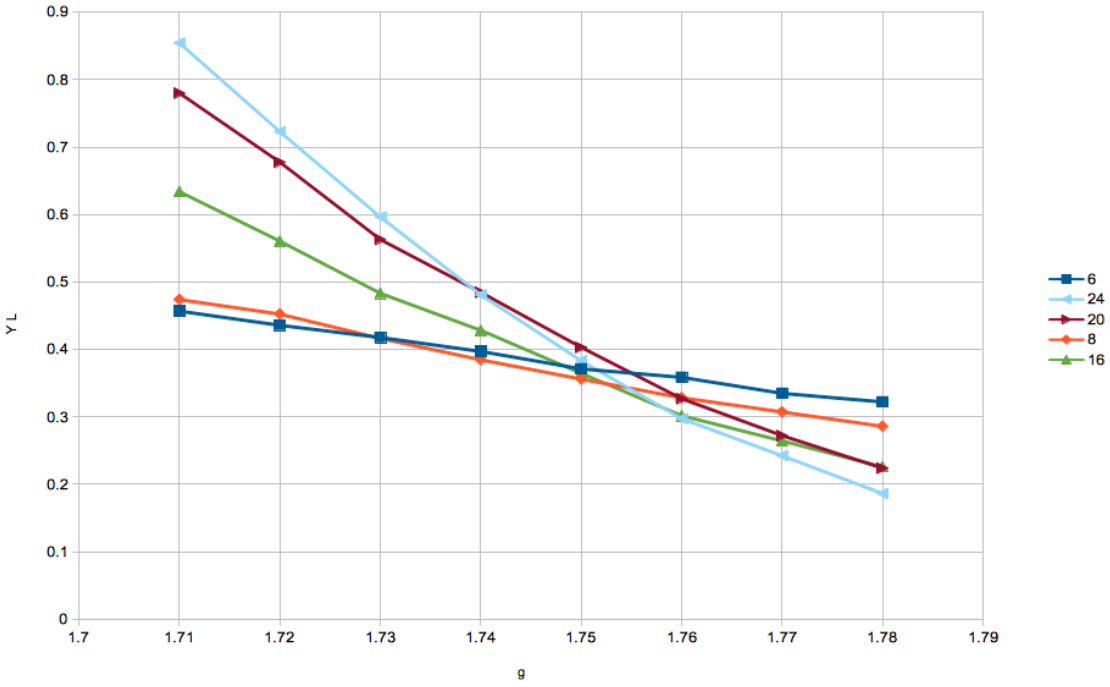

Figure 2.5: Zoomed-in helicity modulus near crossing point for the critical exponent $z = 1.45$, and dilution $p = 2/7$. Lines correspond to different linear size L of the lattice. This yields the estimate for $g_c = 1.76 \pm 0.02$.

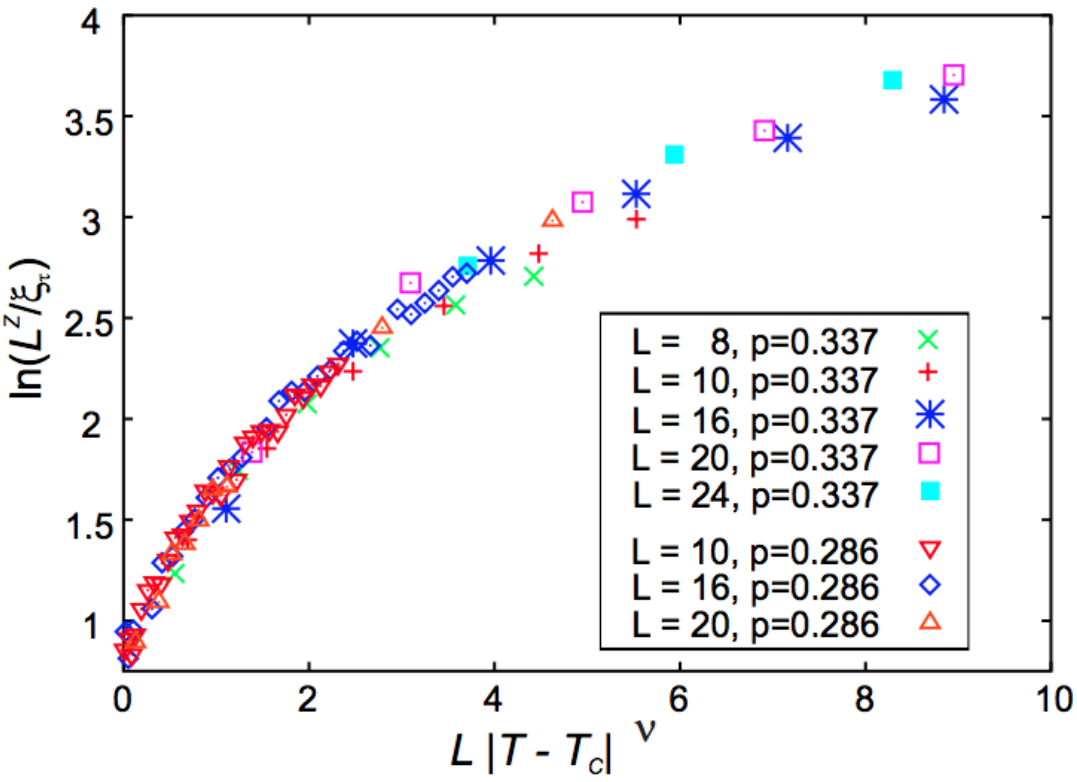

Figure 2.6: Scaling plot of the correlation length ξ_τ in imaginary time direction. Shown are data for two dilutions p, several system sizes L, and temperatures T on the disordered side of the transition. The statistical errors are about one symbol size.

dilutions $p = 2/7 \approx 0.286$ and $p = 0.337$. The system sizes ranged from $L = 8$ to 24 with L_τ fixed as $L_\tau = L^z$ using the dynamical exponent $z = 1.45$ close to one found in [41].

Correlation length ξ_τ in imaginary time direction is equivalent to the inverse energy gap of the corresponding quantum model. We analyze it on the disordered side of the phase transition. The reduced correlation length ξ_τ/L_τ has a scale dimension zero, so the scaling form for samples of shape $L_\tau = L^z$ can be written as $\xi_\tau = L^z F(rL^{1/\nu}, 1)$. Thus we can plot ξ_τ/L^z vs. $(T - T_c)L^{1/\nu}$, the data for different sizes and temperatures should also fall onto a single curve. Fig. 2.6 shows the resulting curve for $z = 1.45$ and $\nu = 1.16$, which is confirming the

critical exponents our collaborators found in [41].

Chapters 2 contains material from the paper: T. Vojta, J. Crewse, M. Puschmann, D. Arovas, and Y. Kiselev, "Quantum critical behavior of the superfluid-Mott glass transition", *Physical Review B*, 94, 134501, (2016). The dissertation author was a co-author of this paper.

Chapter 3

Sp(N) models

One of the ways to gain additional insight about a given quantum spin system is to generalize the spin symmetry group SU(2) to different groups, for example to SU(N) or symplectic group Sp(N) and then study their large-N limit. While SU(N) groups usually are used to study ferromagnets and bipartite antiferromagnets, Sp(N) groups can be used for any antiferromagnet.

3.1 Introduction

Let's motivate the use of a symplectic group to study antiferromagnets. We will use Schwinger bosons representations for the spins. For standard spin group SU(2) one can use two bosons a and b to represent the spin algebra

$$S^+ = a^\dagger b, \;\; S^- = b^\dagger a, \;\; S^z = \tfrac{1}{2}(a^\dagger a - b^\dagger b),$$

together with the occupation constraint that determines the representation of SU(2)

$$a^\dagger a + b^\dagger b = 2S.$$

For the SU(N) case it's possible to use N flavors of the bosons for the natural generalization

$$S_{\mu\nu} = b^\dagger_\mu b_\nu,$$

so that the SU(N) commutation relations are satisfied with the occupancy constraint

$$\sum_{\mu=1}^{N} b^\dagger_\mu b_\mu = n_b.$$

The only bilinear coupling between sites with the same representation that remains unchanged during SU(N) rotations is 'ferromagnetic' coupling

$$-(b^\dagger_{i\alpha} b_{k\alpha})(b^\dagger_{k\beta} b_{i\beta})$$

which is at minimum if the spins on sites i and k are aligned. If the sign in front is reversed, the spins might point in any two different directions to achieve minimum energy. Hence, SU(N) description is not well-suited for the antiferromagnetic case. Only for the bipartite lattice we can artificially inverse spins in one of the two sublattices and then use ferromagnetic interaction for the SU(N) spins to describe antiferromagnetic case. These complications are absent for the Sp(N) group, as first discovered by Sachdev and Read in [42].

We require any two spins to be transformed by the same representation and that there exists a combination of the two that transforms like a singlet. For SU(2), expression $\epsilon^{\alpha\beta} b^\dagger_{i\alpha} b^\dagger_{k\beta}$ transforms like a singlet. Generalization to Sp(N) group would be

$$J^{\alpha\beta} b^\dagger_{i\alpha} b^\dagger_{k\beta},$$

which is a singlet. Here

$$J = \begin{pmatrix} 0 & 1 & & & & \\ -1 & 0 & & & & \\ & & 0 & 1 & & \\ & & -1 & 0 & & \\ & & & & \cdots & \\ & & & & & \cdots \end{pmatrix}$$

and Sp(N) is a group of $2N \times 2N$ unitary matrices U that obey

$$U^T J U = J. \tag{3.1}$$

For the antiferromagnetic system we want to maximize number of singlets $J^{\alpha\beta} b^\dagger_{i\alpha} b^\dagger_{k\beta}$ formed between neighboring sites, and this can be achieved by the following Hamiltonian

$$H = -\tfrac{J}{2N} \sum_{\langle i,j \rangle} (\epsilon^{\alpha\beta} b^\dagger_{im\alpha} b^\dagger_{jm\beta})(\epsilon^{\gamma\delta} b_{in\gamma} b_{jn\delta}). \tag{3.2}$$

A paper by Thernyshov and Sondhi, [43] discusses the case of the SU(N) groups. The Hamiltonian for that case is a ferromagnetic analog of the group

Sp(N)

$$H_{FM} = -\frac{J}{2N}\sum_{\langle i,j\rangle}(b^{\dagger}_{i\alpha}b_{j\alpha})(b^{\dagger}_{j\beta}b_{i\beta}). \tag{3.3}$$

They were studying a finite-temperature transition between a perfectly paramagnetic state and a paramagnetic state with a finite correlation length at $N = \infty$. For the square lattice they found that the transition between mean-field parameter $Q = 0$ and $Q \neq 0$ is discontinuous and takes place at $T_c > 1$. Also they are studying the case of finite, but large N. We will limit ourselves to the case $N = \infty$ and will add to the consideration possible transition to the Bose-Einstein condensate phase.

3.2 Theory

The Sp(N) system that we study is a bosonic generalization of the Heisenberg antiferromagnet

$$H = -\frac{J}{2N}\sum_{\langle i,j\rangle}(\epsilon^{\alpha\beta}b^{\dagger}_{im\alpha}b^{\dagger}_{jm\beta})(\epsilon^{\gamma\delta}b_{in\gamma}b_{jn\delta}), \tag{3.4}$$

where $m, n \in \{1, \ldots, N\}$ and $\alpha, \beta, \gamma, \delta \in \{1, 2\}$. The representation of Sp(N) is fixed by the constraint $\sum_{m,\alpha} b^{\dagger}_{im\alpha}b_{im\alpha} = n_b$ for each i. This is imposed by a Lagrange multiplier λ_i at each site i. The Euclidian Lagrangian is

$$L_E = \sum_{im\alpha}\overline{b}_{im\alpha}\partial_\tau b_{im\alpha} + i\sum_i \lambda_i(\overline{b}_{im\alpha}b_{im\alpha} - n_b) - \frac{J}{2N}\sum_{\langle i,j\rangle}(\epsilon^{\alpha\beta}\overline{b}_{im\alpha}\overline{b}_{jm\beta})(\epsilon^{\gamma\delta}b_{in\gamma}b_{jn\delta}), \tag{3.5}$$

Let's define $K = n_b/2N$. For Sp(1) $\simeq$ SU(2), $N = 1$ and $K = \frac{1}{2}n_b = S$, the

spin quantum number. Let $b_{im\alpha} \equiv \sqrt{K} z_{im\alpha}$, so

$$L_E = K \sum_{im\alpha} \overline{z}_{im\alpha} \partial_\tau z_{im\alpha} + iK \sum_i \lambda_i (\overline{z}_{im\alpha} z_{im\alpha} - n_b) - \frac{JK^2}{2N} \sum_{\langle i,j \rangle} (\epsilon^{\alpha\beta} \overline{z}_{im\alpha} \overline{z}_{jm\beta})(\epsilon^{\gamma\delta} z_{in\gamma} z_{jn\delta}). \tag{3.6}$$

Now we invoke Hubbard-Stratanovich transformation:

$$-\tfrac{JK^2}{2N} |R_{ij}|^2 \to \tfrac{2N}{JK^2} |Q_{ij}|^2 - Q_{ij} \overline{R}_{ij} - \overline{Q}_{ij} R_{ij}, \tag{3.7}$$

where initial expression is restored for $Q_{ij} = \frac{JK^2}{2N} R_{ij}$. So we have

$$\begin{aligned} L_E = K \sum_{im\alpha} \overline{z}_{im\alpha} \partial_\tau z_{im\alpha} + \tfrac{2N}{JK^2} \sum_{\langle i,j \rangle} |Q_{ij}|^2 + \sum_i \mu_i (\overline{z}_{im\alpha} z_{im\alpha} - 2N) \\ - \sum_{\langle i,j \rangle} (Q_{ij} \epsilon^{\alpha\beta} \overline{z}_{im\alpha} \overline{z}_{jm\beta} + \overline{Q}_{ij} \epsilon^{\alpha\beta} z_{im\alpha} z_{jm\beta}), \end{aligned} \tag{3.8}$$

where $\mu_i = iK\lambda_i$. We may further adimensionalize, writing $Q_{ij} \to JK^2 Q_{ij}$, $\mu_i \to JK^2 \mu_i$, $T \to JK^2 \Theta$, and $\tau \to \frac{1}{JK^2} \sigma$. The Euclidian action is then

$$\begin{aligned} S_E = \int_0^{\Theta^{-1}} \mathrm{d}\sigma \{ K \sum_{im\alpha} \overline{z}_{im\alpha} \partial_\sigma z_{im\alpha} + 2N \sum_{\langle i,j \rangle} |Q_{ij}|^2 + \sum_i \mu_i (\overline{z}_{im\alpha} z_{im\alpha} - 2N) \\ - \sum_{\langle i,j \rangle} (Q_{ij} \epsilon^{\alpha\beta} \overline{z}_{im\alpha} \overline{z}_{jm\beta} + \overline{Q}_{ij} \epsilon^{\alpha\beta} z_{im\alpha} z_{jm\beta}) \}. \end{aligned} \tag{3.9}$$

One of the ways to take the limit $N \to \infty$ is to keep $K = n_b/2N$ fixed. This approach for SU(N) case was discussed by Arovas and Auerbach [44]. We will consider easier $K \to \infty$ limit for the Sp(N) spin group, as for SU(N) group $K \to \infty$ limit was studied by Thernyshov and Sondhi [43].

We must have $z_{im\alpha}(\sigma)$ independent of σ so that the action does not blow

up. So we conclude $S_E = E/\Theta$, with

$$E = 2N \sum_{\langle i,j \rangle} |Q_{ij}|^2 - \sum_{\langle i,j \rangle} (Q_{ij} \epsilon^{\alpha\beta} \overline{z}_{ima} \overline{z}_{jm\beta} + \overline{Q}_{ij} \epsilon^{\alpha\beta} z_{ima} z_{jm\beta}) + \sum_i \mu_i (\overline{z}_{ima} z_{ima} - 2N) \tag{3.10}$$

The mean-field equations are

$$\frac{\partial \langle E \rangle}{\partial \overline{Q}_{ij}} = 0 = 2N Q_{ij} - \sum_m \epsilon^{\alpha\beta} \langle z_{ima} z_{jm\beta} \rangle, \tag{3.11}$$

and

$$\frac{\partial \langle E \rangle}{\partial \mu_i} = 0 = \sum_i \langle \overline{z}_{ima} z_{ima} \rangle - 2N. \tag{3.12}$$

The flavor index drops out of the calculations, so we have a free energy per flavor of

$$\frac{F}{N} = 2 \sum_{\langle i,j \rangle} |Q_{ij}|^2 - 2 \sum_i \mu_i - \Theta \ln \int D[\overline{z}, z] \exp\{-\tfrac{1}{2\Theta} \begin{pmatrix} \overline{z} & z \end{pmatrix} M \begin{pmatrix} z \\ \overline{z} \end{pmatrix}\}, \tag{3.13}$$

where

$$M_{i\alpha, j\beta} = \begin{pmatrix} \mu_i \delta_{ij} \delta_{\alpha\beta} & -Q_{ij} \epsilon^{\alpha\beta} \\ -\overline{Q}_{ij} \epsilon^{\alpha\beta} & \mu_i \delta_{ij} \delta_{\alpha\beta}. \end{pmatrix} \tag{3.14}$$

Note that $M = M^\dagger$ and $Q_{ji} = -Q_{ij}$ is nonzero only for i, j nearest neighbors. By substituting

$$\tfrac{1}{2\Theta} \begin{pmatrix} \overline{z} & z \end{pmatrix} M \begin{pmatrix} z \\ \overline{z} \end{pmatrix} = \tfrac{1}{\Theta} \begin{pmatrix} X & Y \end{pmatrix} U^\dagger M U \begin{pmatrix} X \\ Y \end{pmatrix} \tag{3.15}$$

with

$$U = \tfrac{1}{\sqrt{2}} \begin{pmatrix} 1 & i \\ 1 & -i \end{pmatrix} \tag{3.16}$$

Thus,

$$\frac{F}{N} = 2\sum_{\langle i,j\rangle}|Q_{ij}|^2 - 2\sum_i \mu_i + \frac{\Theta}{2}\,\mathrm{Tr}\,\ln\frac{M}{\Theta}. \tag{3.17}$$

The mean-field equations are (without summing over i)

$$Q_{ij} = \tfrac{1}{2}\epsilon^{\alpha\beta}\langle z_{i\alpha} z_{j\beta}\rangle, \tag{3.18}$$

$$1 = \tfrac{1}{2}\langle \overline{z}_{i\alpha} z_{i\alpha}\rangle. \tag{3.19}$$

Solving the mean-field conditions gives us the same result as for ferromagnetic SU(N) case in Ref. [43]

$$\mu_i - \sum_k |Q_{ik}|^2 = \Theta. \tag{3.20}$$

Now, after expanding the free energy in powers of Q we get

$$\frac{F}{N} = (1-\tfrac{1}{\Theta})\sum_i |Q_{ii}|^2 + \tfrac{1}{\Theta^3}\sum_i (QQ^\dagger)^2_{ii} - \tfrac{1}{2\Theta^3}\sum_{ijkl}(Q_{ij}Q^\dagger_{jk}Q_{kl}Q^\dagger_{li}) + \ldots \tag{3.21}$$

For the uniform state $Q_{ij} = Qe^{i\theta_{ij}}A_{ij}$, where A_{ij} is an antisymmetric adjacency matrix, $A_{ij} = \pm 1$ only for nearest neighbors and

$$\tfrac{1}{N_s}\sum_i (QQ^\dagger)_{ii} = zQ^2$$

$$\tfrac{1}{N_s}\,\mathrm{Tr}\,(QQ^\dagger QQ^\dagger) = z(2z-1)Q^4 + l_4 Q^4\cos\phi_4$$

with $e^{i\phi_4} = e^{i(\theta_{ij}-\theta_{jk}+\theta_{kl}-\theta_{li})}$ and l_4 is the number of the loops of length 4. So

$$\frac{F}{NN_s} = (1-\tfrac{1}{\Theta})zQ^2 + \tfrac{1}{2\Theta^3}(z - l_4\cos\phi_4)Q^4 + \dots \tag{3.22}$$

We should note that the free energy agrees with the ferromagnetic SU(N) case for bipartite lattices, where there are no odd-length loops.

3.3 Condensate field

One of the possible phases of Sp(N) system is the Bose-Einstein condensate. We are studying the conditions needed for this phase to appear by adding fictional field ν, which we will remove later.

$$\Delta H = -\sqrt{N_s}\sum_{i,m,\alpha}(\nu_{i\alpha}b^\dagger_{im\alpha} + \overline{\nu}_{i\alpha}b_{im\alpha}), \tag{3.23}$$

where Shwinger bosons $b_{im\alpha} = \sqrt{K}z_{im\alpha}$. After rescaling and the Legendre transformation to the new variables $\psi_{i\alpha}$ we get

$$g(Q,\mu,\psi,\Theta) = 2\sum_{\langle i,j,\rangle}|Q_{ij}|^2 - 2\sum_i \mu_i + \tfrac{\Theta}{2}\operatorname{Tr}\ln\tfrac{M}{\Theta} + \tfrac{1}{2}\begin{pmatrix}\overline{\psi}_{i\alpha} & \psi_{i\alpha}\end{pmatrix}M_{i\alpha,j\beta}\begin{pmatrix}\psi_{j\beta}\\ \overline{\psi}_{j\beta}\end{pmatrix}$$

and $\frac{\partial g}{\partial\overline{\psi}_{i\alpha}} = \nu_{i\alpha}$, so

$$\begin{pmatrix}\nu & \overline{\nu}\end{pmatrix} = M\begin{pmatrix}\psi_{j\beta}\\ \overline{\psi}_{j\beta}\end{pmatrix}, \tag{3.24}$$

where

$$M = \begin{pmatrix}\mu\otimes\mathbb{1} & -Q\otimes\epsilon\\ -Q^*\otimes\epsilon & \mu\otimes\mathbb{1}\end{pmatrix} \tag{3.25}$$

and if we call $\mu_{i\alpha,j\beta} = \mu_i \delta_{ij} \delta_{\alpha\beta}$ and $R_{i\alpha,j\beta} = Q_{ij}\epsilon^{\alpha\beta}$, then $\mu = \mu^T$ and $R = R^T$,

$$M^{-1} = \begin{pmatrix} A \otimes \mathbb{1} & B \otimes \epsilon \\ B^* \otimes \epsilon & A^* \otimes \mathbb{1} \end{pmatrix}, \tag{3.26}$$

where

$$A\mu - BR^\dagger = \mathbb{1}, \qquad B^\dagger \mu - AR^\dagger = 0$$
$$-AR + B\mu = 0, \qquad -B^\dagger R + A\mu = \mathbb{1}$$

with $A = A^\dagger$, $B = -B^T$. Including the condensate, the mean-field equations become

$$\frac{\delta g}{\delta \mu_i} = 0 = 2(\Theta A_{ii} - 1) + \sum_\alpha |\psi_{i\alpha}|^2 \tag{3.27}$$

$$\frac{\delta g}{\delta \overline{Q}_{ij}} = 0 = Q_{ij} - \Theta B_{ij} - \tfrac{1}{2}\epsilon^{\alpha\beta}\psi_{i\alpha}\psi_{j\beta}, \tag{3.28}$$

so

$$1 = \Theta A_{ii} + \tfrac{1}{2}\sum_\alpha |\psi_{i\alpha}|^2 \tag{3.29}$$

$$Q_{ij} = \Theta B_{ij} + \tfrac{1}{2}\epsilon^{\alpha\beta}\psi_{i\alpha}\psi_{j\beta}. \tag{3.30}$$

Note also $\frac{\partial g}{\partial \overline{\nu}_{i\alpha}} = \psi_{i\alpha} - \langle z_{i\alpha}\rangle = 0$, so $\psi_{i\alpha} = \langle z_{i\alpha}\rangle$ is the condensate. Finally we can see that if $\nu = \overline{\nu} = 0$, then either $\psi = \overline{\psi} = 0$ or M has a zero eigenvalue. From the equations 3.29 and 3.30 we can see that

$$(1 - \tfrac{1}{2}\sum_\alpha |\psi_{i\alpha}|^2)\mu_i = \Theta + \sum_k |Q_{ik}|^2 + \tfrac{1}{2}\epsilon^{\alpha\beta} Q_{ik}\overline{\psi}_{k\alpha}\overline{\psi}_{i\beta}. \tag{3.31}$$

If $\psi \neq 0$, then we must have

$$\mu_i \psi_{i\alpha} - Q_{ij}\epsilon_{\alpha\beta}\overline{\psi}_{j\beta} = 0, \tag{3.32}$$

thus

$$\epsilon^{\alpha\beta} Q_{ik}\overline{\psi}_{k\alpha} = -\epsilon_{\beta\alpha} Q_{ik}\overline{\psi}_{k\alpha} = -\psi_{i\beta}, \tag{3.33}$$

and therefore

$$\mu_i = \Theta + \sum_k |Q_{ik}|^2. \tag{3.34}$$

The condensation temperature is set by $\psi = \overline{\psi} = 0$ and requiring that M has a zero eigenvalue.

If $\psi = \overline{\psi} = 0$, then $\mu_i = \Theta + \sum_j |Q_{ij}|^2$, which is the same as for ferromagnetic SU(N) case. Free energy to the first non-zero order in Q becomes

$$f = -2N_s\Theta + (1 - \tfrac{1}{\Theta}) \sum_{i,j} |Q_{ij}|^2 + \ldots \tag{3.35}$$

This establishes that any *continuous* transition to $Q_{ij} \neq 0$ must take place at $\Theta_c = 1$. For $\Theta > \Theta_c$, $Q_{ij} = 0$ and the response is purely local.

3.4 Cubic lattice

In the uniform Q case we may have three phases, $Q_{ij} = 0$ phase, $Q_{ij} \neq 0$, and the condensate phase. We will determine which of the three is preferred on the regular cubic lattice.

Free energy

$$g = 2\sum_{i,j}|Q_{ij}|^2 - 2\sum_i \mu_i + \tfrac{T}{2}\,\mathrm{Tr}\,\ln M/T + \tfrac{1}{2}\begin{pmatrix}\overline{\psi}_{i\alpha} & \psi_{i\alpha}\end{pmatrix} M_{i\alpha,j\beta}\begin{pmatrix}\psi_{j\beta}\\ \overline{\psi}_{j\beta}\end{pmatrix}. \tag{3.36}$$

Taking account equation 3.26, and mean-field equations 3.29 and 3.30, and calling again dimensionless temperature $T \equiv \Theta$,

$$\mu_i = T + \sum_j |Q_{ij}|^2 \tag{3.37}$$

and

$$\begin{aligned}\delta g = \sum_i (2TA_{ii} - 2 + \sum_\alpha |\psi_{i\alpha}|^2)\delta\mu_i + \sum_{i,j}(Q^*_{ij} - TB^*_{ij} - \tfrac{1}{2}\epsilon^{\alpha\beta}\overline{\psi}_{i\alpha}\overline{\psi}_{j\beta})\delta Q_{ij} \\ + \sum_{i,j}(Q_{ij} - TB_{ij} - \tfrac{1}{2}\epsilon^{\alpha\beta}\psi_{i\alpha}\psi_{j\beta})\delta Q^*_{ij} + \sum_{i,\alpha}(\overline{\nu}_{i\alpha}\delta\psi_{i\alpha} + \nu_{i\alpha}\delta\overline{\psi}_{i\alpha})\end{aligned} \tag{3.38}$$

we can calculate it switching to the reciprocal momentum space

$$Q_{\vec{R}a,\vec{R}'b} = \tfrac{1}{N_c}\sum_{\vec{k}} Q_{ab}(\vec{k})e^{i\vec{k}(\vec{R}-\vec{R}')}. \tag{3.39}$$

where N_c is the number of cells, $\vec{R},\vec{R}'$ are Bravais lattice vectors, and a,b are basis labels. Also

$$M_{\vec{R}a\alpha,\vec{R}'b\beta} = \tfrac{1}{N_c}\sum_{\vec{k}} e^{i\vec{k}(\vec{R}-\vec{R}')}N_{a\alpha,b\beta}(\vec{k}), \tag{3.40}$$

where

$$N_{a\alpha,b\beta}(\vec{k}) = \begin{pmatrix}\mu_a\delta_{ab}\delta\alpha\beta & -Q_{ab}(\vec{k})\epsilon_{\alpha\beta}\\ Q^*_{ba}(\vec{k})\epsilon_{\alpha\beta} & \mu_a\delta_{ab}\delta\alpha\beta\end{pmatrix} \tag{3.41}$$

For the cubic lattice number of basis sites is one, $Q(-\vec{k}) = -Q(\vec{k})$, and

$$N(\vec{k}) = \begin{pmatrix} \mu & 0 & 0 & -Q(\vec{k}) \\ 0 & \mu & Q(\vec{k}) & 0 \\ 0 & Q^*(\vec{k}) & \mu & 0 \\ -Q^*(\vec{k}) & 0 & 0 & \mu \end{pmatrix} \tag{3.42}$$

and $\det N(\vec{k}) = (\mu^2 - |Q(\vec{k})|^2)^2$.

We can write $Q(\vec{k}) = Q\gamma(\vec{k})$ and $\gamma(\vec{k}) = \sum_\nu 2i \sin(\vec{k} \cdot \vec{a}_\nu)$. Equations can be simplified with the help of $\zeta(\vec{\theta}) = \frac{1}{d}\sum_{a=1}^{d} \sin\theta_a \in [-1, 1]$ and

$$D_d(\zeta) \equiv \int \frac{d^d\theta}{(2\pi)^d} \delta(\zeta - \zeta(\vec{\theta})), \tag{3.43}$$

which is a density of states for d-dimensional lattice. For three-dimensional cubic lattice density of states is shown on the Fig. 3.1.

We will consider three following phases. Phase A is a totally paramagnetic phase, $Q_{ij} = 0$, so $\mu_i = T$, $\psi_i \alpha = 0$, so

$$g_A = -2T. \tag{3.44}$$

Phase B will have order parameter $Q \neq 0$, so $\mu = T + 2dQ^2$, but no condesate: $\psi = 0$, so

$$g_B = 2dQ^2 - 2\mu + T\int_{-1}^{1} \mathrm{d}\zeta D_d(\zeta) \ln \frac{\mu^2 - 4d^2Q^2\zeta^2}{T^2}. \tag{3.45}$$

In this case order parameter Q is determined from mean-field equatiion

$$1 = \int_{-1}^{1} \mathrm{d}\zeta D_d(\zeta) \frac{T\mu}{\mu^2 - 4d^2Q^2\zeta^2}, \tag{3.46}$$

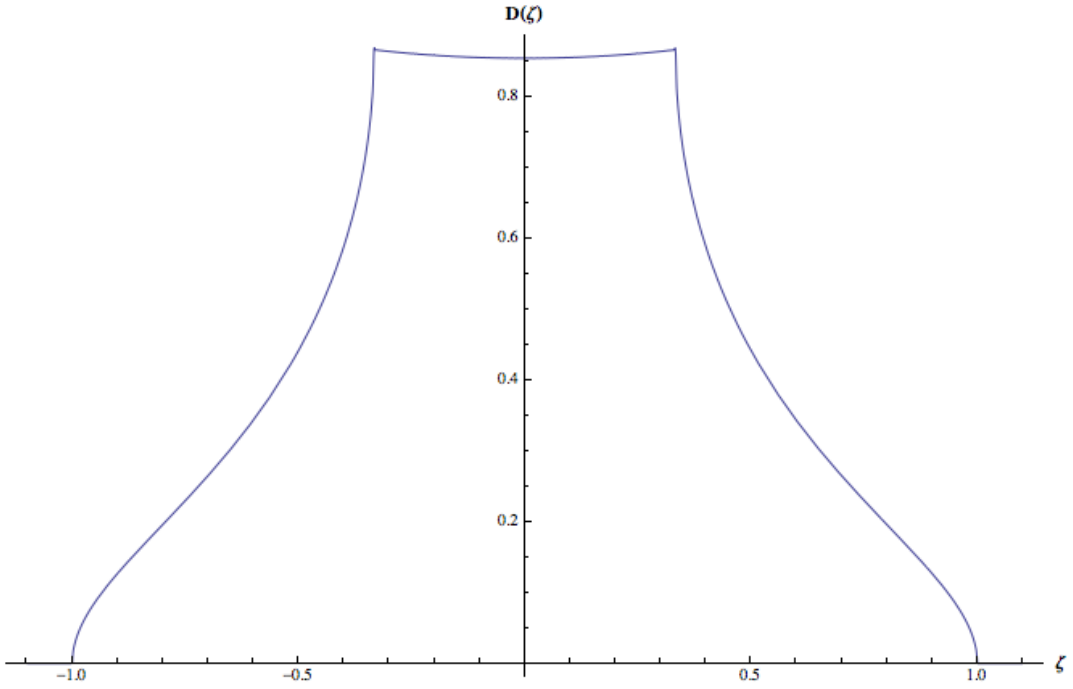

Figure 3.1: Density of states as a function of $\zeta(\vec{\theta}) = \frac{1}{3}\sum_{a=1}^{3}\sin\theta_a$.

or equivalently, taking into account that $\mu = T + 2dQ^2$,

$$1 = T\int_{-1}^{1} \mathrm{d}\zeta D_d(\zeta)\frac{1}{T-2dQ\zeta+2dQ^2}. \tag{3.47}$$

Phase C is a condensate phase, so $\psi \neq 0$, and matrix M has a zero eigenvalue, so $\mu = 2dQ$. Then free energy

$$g_C = 2dQ(Q-2) + T\int_{-1}^{1} \mathrm{d}\zeta D_d(\zeta)\ln(1-\zeta^2) + 2T\ln 2dQ/T. \tag{3.48}$$

Mean-field equations become

$$1 = \frac{T}{2dQ}\int_{-1}^{1} \mathrm{d}\zeta \frac{D_d(\zeta)}{1-\zeta^2} + \frac{1}{2}|\psi|^2 \tag{3.49}$$

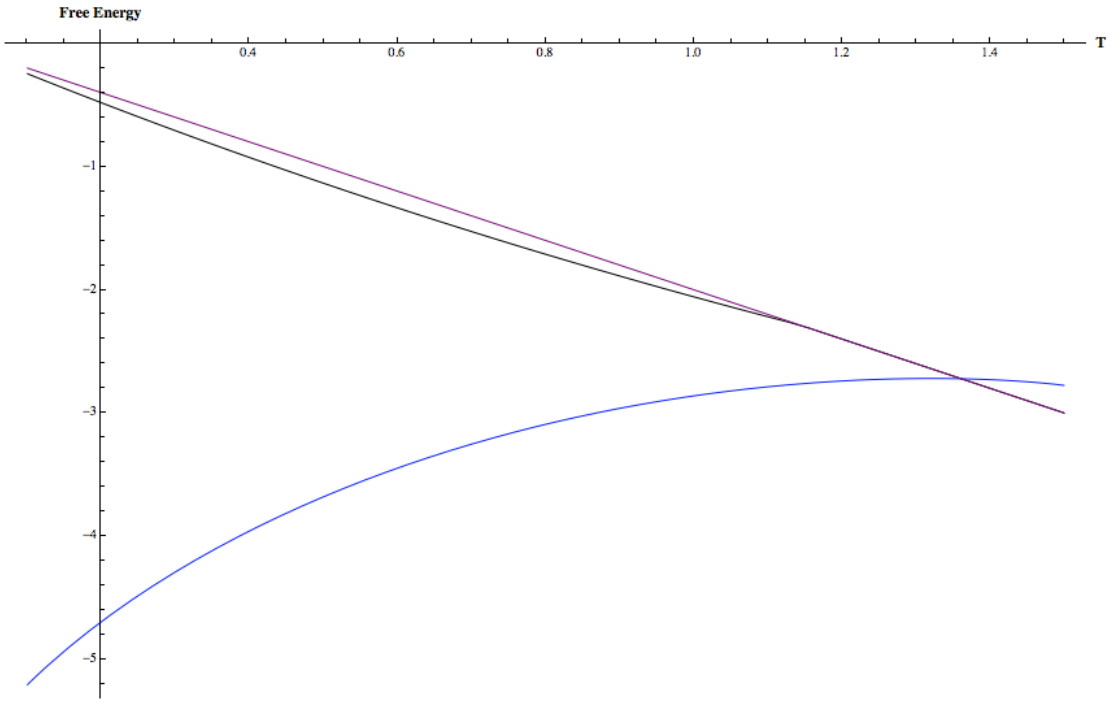

Figure 3.2: Dimensionless free energies for the three possible phases g_A,g_B, and g_C corresponding to the pink, black and blue respectively.

and

$$\frac{\partial g}{\partial Q} = 0 = 4d(Q-1) + \frac{2T}{Q} = 0, \tag{3.50}$$

so $Q(Q-1) + \frac{T}{2d} = 0$ and so $Q = \frac{1}{2} + \sqrt{\frac{1}{4} - \frac{T}{2d}}$. So there is no solution for $T > d/2$.

To determine the phase for each temperature we take $d = 3$ for the cubic lattice, numerically calculate $D_3(\zeta)$ and compare g_A, g_B, and g_C. For each given temperature the system will be in the phase that corresponds to the minimum of the three free energies. The result is summarized in the Fig. 3.2. We can see that for high temperatures the system is in paramagnetic phase (phase A, pink curve). When the temperature is lowered, the Bose-Einstein condensate appears (phase C, blue curve). Free energy for the phase B (black curve) coincides with the phase A (pink curve) for temperatures $T > 1.16 \pm 0.01$, as for that temperatures the order parameter $Q = 0$ for the phase B (see Fig. 3.3), which makes phase B

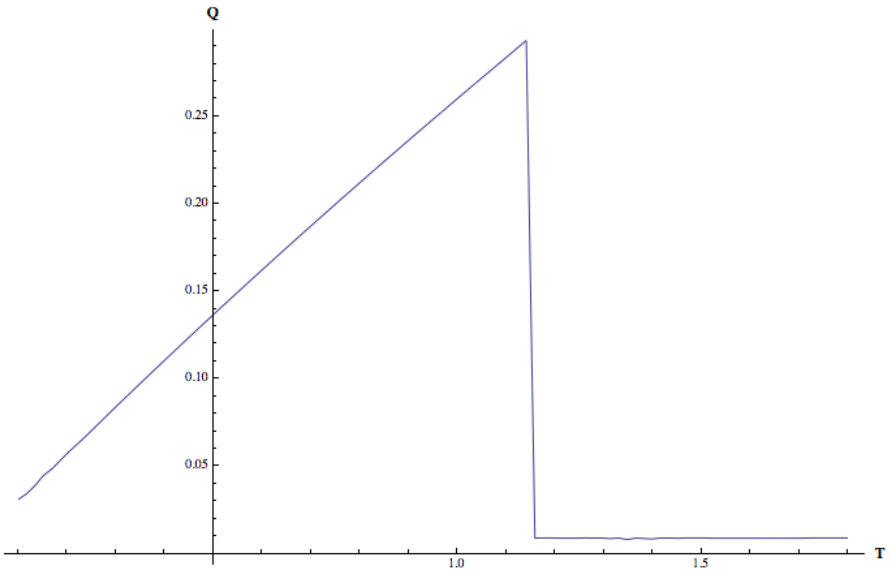

Figure 3.3: Temperature dependence of the order parameter Q for the phase B.

identical to the phase A.

These results indicate that three-dimensional antiferromagnetic system under consideration does not have the extra phase found in the work [43], where the ferromagnetic case was studied. In the ferromagnetic case there is a finite-temperature phase transition between a perfect paramagnet ($Q = 0$) and a paramagnetic state with a finite correlation length, that is absent in the SU(2) case and hence is considered an artifact of the large-N SU(N) approach. For our antiferromagnetic Sp(N) case the same transition is absent. Instead, we found a transition between the perfect paramagnet ($Q = 0$) and a condensed phase that corresponds to a long-range order present in the system.

Chapter 3 contains material currently being prepared for submission for publication: Y.Y. Kiselev and D.P. Arovas, "Large-N limit and phase transitions of two-dimensional Sp(N) magnets". The dissertation author was the primary investigator and author of this work.

Chapter 4

Floquet systems

Properties of the many-body systems subject to periodic driving are interesting from the fundamental point of view. Such systems may support unusual phases of matter, for example, phases with non-trivial topological properties and robust edge modes.

Let's consider a system that is driven periodically with period T:

$$H(t+T) = H(t), \tag{4.1}$$

and the evolution operator for the whole period is

$$U(T) = \mathrm{T}\exp\left(-\tfrac{i}{\hbar}\int_0^T \mathrm{d}t' H(t')\right), \tag{4.2}$$

where T orders earlier times to the right. This evolution operator has eigenvalues $e^{i\omega_\alpha}$, and ω_α are called quasi-energies:

$$U(T)\left|\psi_\alpha\right\rangle = e^{i\omega_\alpha}\left|\psi_\alpha\right\rangle, \tag{4.3}$$

where $\left|\psi_\alpha\right\rangle$ is a Floquet eigenstate. Evolution for a part of the period is given by the truncated evolution operator

$$U(t) = \mathrm{T}\exp\left(-\tfrac{i}{\hbar}\int_0^t \mathrm{d}t' H(t')\right), \tag{4.4}$$

and starting with a given Floquet eigenstate $\left|\psi_\alpha\right\rangle$, average of some operator $\hat{O}$ over a cycle is

$$\langle \hat{O}_\alpha \rangle_T = \tfrac{1}{T}\int_0^T \mathrm{d}t \left\langle \psi_\alpha \middle| U^\dagger(t)\,\hat{O}\,U(t) \middle| \psi_\alpha \right\rangle, \tag{4.5}$$

4.1 Non-interacting Floquet systems

We are considering system of fermions on two-dimensional square lattice. Our system will have hopping 'enabled' along particular nearest-neighbor links of the lattice, depending on time. This setup is similar to the approach of Titum et al. in [45]. The Hamiltonian is periodic, with the period $T = \sum_{n=1}^{4} T_n$, where the time segments T_1, T_2, T_3 and T_4 correspond to links allowed for hopping, see Fig. 4.1. In the work [45] all time segments were the same length, and additionally there was an onsite disorder potential acting during the same time segment $T/5$. Their system allows for a phase with a peculiar topological properties: all bulk Floquet states are localized, but the system still hosts topologically-protected chiral modes at the edges.

In our system there is going to be no disorder, but time segments T_1, T_2, T_3 and T_4 will be different from each other. We divide the system into two sublattices, A and B. During n-th time segment that lasts T_n seconds the

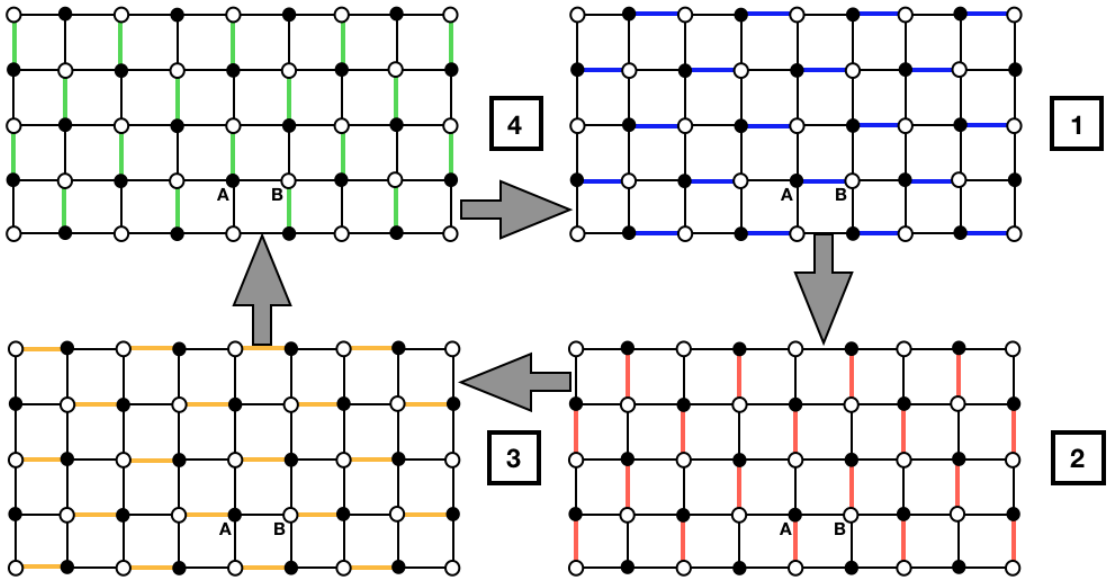

Figure 4.1: Engaged links for time segments 1,2,3 and 4.

Hamiltonian is

$$H_n = \theta \sum_{\langle i,j\rangle \in \Lambda_n} (b_i^\dagger a_j + a_j^\dagger b_i) + \lambda\theta \sum_{\langle i,j\rangle} b_i^\dagger b_i a_j^\dagger a_j, \tag{4.6}$$

where a_i and b_j are annihilation operators for sublattices A and B, Λ_n denotes enabled edges for time segment T_n and λ controls density-density interactions between all neighboring sites, independent of the current time.

The evolution operator for one period T is

$$U(T) = U_4 U_3 U_2 U_1, \tag{4.7}$$

where $U_n = e^{-i\frac{T_n}{\hbar}H_n}$.

4.2 Mean-field solution and its properties

We are going to find approximate solution for the problem above by using mean-field theory. Interaction terms of the Hamiltonian during segment T_n

$$b_i^\dagger b_i a_j^\dagger a_j \approx \tfrac{1}{2}(\mu_n^b b_i^\dagger b_i + \mu_n^a a_j^\dagger a_j), \tag{4.8}$$

where

$$\begin{aligned} \mu_n^a &= \langle b_i^\dagger b_i \rangle_{T_n} \\ \mu_n^b &= \langle a_i^\dagger a_i \rangle_{T_n}. \end{aligned} \tag{4.9}$$

Set of μ_n depends on the average occupation densities on the opposite sublattice during the time segment T_n. We will switch to the momentum space, and the hopping term in $H_i(\boldsymbol{k})$ becomes $\hat{n}_i \cdot \hat{\sigma}$, where $\hat{\sigma} = (\sigma_x, \sigma_y)$ and

$$\begin{aligned} n_1 &= (\cos(k_x), \sin(k_x)) \\ n_2 &= (\cos(k_y), -\sin(k_y)) \\ n_3 &= (\cos(k_x), -\sin(k_x)) \\ n_4 &= (\cos(k_y), \sin(k_y)) \end{aligned} \tag{4.10}$$

We will remove constant term proportional to $\frac{\mu_i^a + \mu_i^b}{2}$ from the Hamiltonian H_n, so our vector

$$\vec{g_i} = \{n_i^x, n_i^y, \lambda(\mu_i^a - \mu_i^b)/2\}, \tag{4.11}$$

and the three-component vector $\vec{n_i} = \vec{g_i}/|\vec{g_i}|$.

The evolution operator for one segment is

$$U_i = \cos(\theta T_i |\vec{g}_i|) \cdot 1 + i \sin(\theta T_i |\vec{g}_i|)(\vec{n}_i \cdot \vec{\sigma}). \tag{4.12}$$

We will use the following procedure to find the self-consistent values of μ_n. First we choose initial eight values for μ_n, which correspond to a half filling state, then find two quasi-energy levels that correspond to the given Floquet evolution operator in momentum space, and fill up the lower level. This approximation is rather crude, and should be regarded as part of the definition of the system in question. We eliminate all constant terms in the Hamiltonian, so the gap may close only at $\omega = 0, \pi$. Lower level band lies below zero, $\omega \in [-\pi, 0]$. Then, it is possible to calculate resulting μ_n, see eq. 4.9, and we repeat the cycle until μ_n do not change anymore.

Numerical results are shown on the picture following. For small $\lambda \lesssim 0.5$ the equilibrium stable solution for the problem corresponds to $\mu_n = 0.5$ for both sublattices and for all time segments. When λ increases, the solution $\mu_n = 0.5$, is no more stable. Instead, there appear two stable solutions when $1 - \mu_n^b = \mu_n^a < 0.5$, or vice versa, as the system is symmetric to the change $\mu_n \to 1 - \mu_n$. Fig. 4.2 shows results for μ_1^a for the case when $\mu_1^a \leq \mu_1^b$. For larger λ or smaller θ, μ_1^a becomes smaller.

The topological index C for the eigenfunction $\left|\psi_{\boldsymbol{k}}\right\rangle$ of the evolution operator is given by

$$C = \frac{1}{4\pi} \int_\Omega \mathrm{d}^2 k \hat{n}_{\boldsymbol{k}} \cdot \frac{\partial \hat{n}_{\boldsymbol{k}}}{\partial k_x} \times \frac{\partial \hat{n}_{\boldsymbol{k}}}{\partial k_y}, \tag{4.13}$$

where Ω denotes the first Brillouin zone. We can approximately evaluate C using

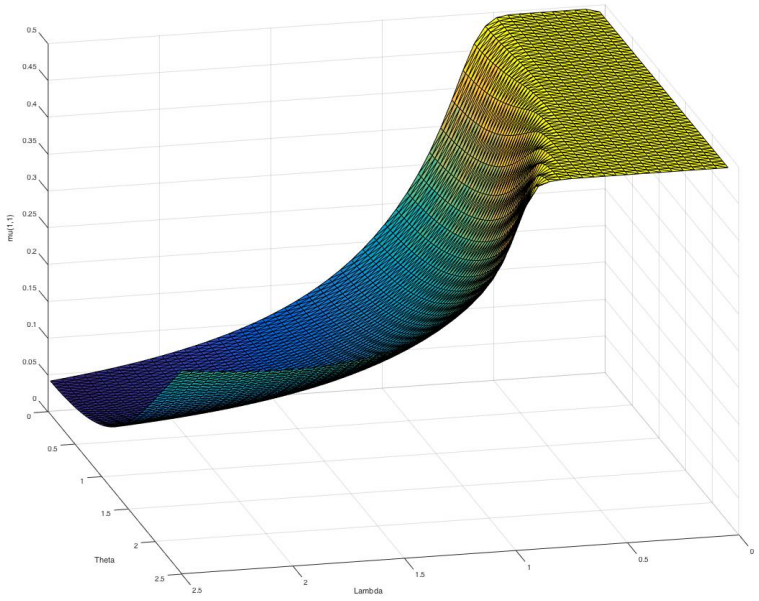

Figure 4.2: Plot of μ_1^a as a function of λ and θ. Time segments are $T_i = T \cdot [0.2, 0.3, 0.4, 0.1]$.

a triangulation of the Brillouin zone, following Sachdev and Park in [46]:

$$C = \frac{1}{2\pi} \sum_{\langle ijk \rangle} \tan^{-1} \left(\frac{\hat{n}_i \cdot \hat{n}_j \times \hat{n}_k}{1 + \hat{n}_i \cdot \hat{n}_j + \hat{n}_j \cdot \hat{n}_k + \hat{n}_k \cdot \hat{n}_i} \right). \tag{4.14}$$

Results are shown in the figure 4.3. Blue region is a zone of $C = 0$, and yellow one is $C = 1$.

We find that even though the analogous system that corresponds to the constant Hamiltonian does not have a topological order, the model that includes time-dependent terms shows topological behavior.

Chapter 4 contains material currently being prepared for submission for publication: Y.Y. Kiselev and D.P. Arovas, “Two and one-dimensional Floquet systems”. The dissertation author was the primary investigator and author of this work.

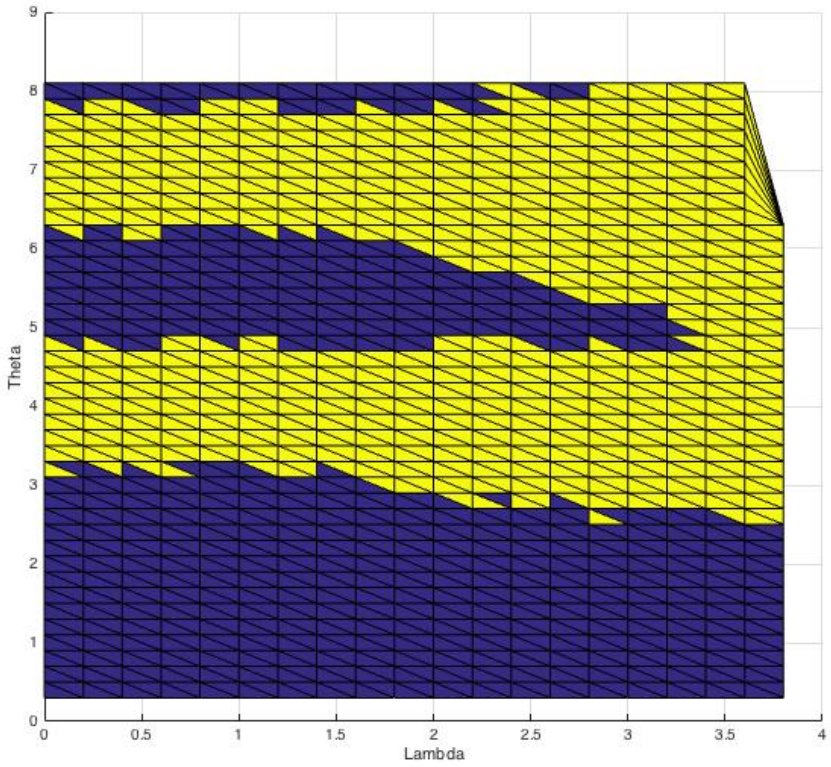

Figure 4.3: Plot of C corresponding to the found combination of μ_n as a function of λ and θ. Time segments are $T_i = T \cdot [0.2, 0.3, 0.4, 0.1]$. Blue region is a zone of $C = 0$, and yellow one is $C = 1$.

Bibliography

[1] J. M. Hopkinson, S. V. Isakov, H.-Y. Kee, and Y. B. Kim, Phys. Rev. Lett. **99**, 037201 (2007).

[2] I. Affleck, T. Kennedy, E. H. Lieb, and H. Tasaki, Comm. Math. Phys. **115**, 477 (1988).

[3] Y. Kiselev, S. Parameswaran, and D. P. Arovas, Journal of Statistical Mechanics: Theory and Experiment **2016**, 013105 (2016).

[4] N. Prokof'ev and B. Svistunov, Physical review letters **87**, 160601 (2001).

[5] I. Affleck, T. Kennedy, E. H. Lieb, and H. Tasaki, Phys. Rev. Lett. **59**, 799 (1987).

[6] F. D. M. Haldane, Physics Letters A **93**, 464 (1983).

[7] F. D. M. Haldane, Phys. Rev. Lett. **61**, 1029 (1988).

[8] H. Yao and S. A. Kivelson, Phys. Rev. Lett. **105**, 166402 (2010).

[9] D. P. Arovas, Physical Review B (Condensed Matter and Materials Physics) **77**, 104404 (2008).

[10] D. P. Arovas, A. Auerbach, and F. D. M. Haldane, Phys. Rev. Lett. **60**, 531 (1988).

[11] S. A. Parameswaran, S. L. Sondhi, and D. P. Arovas, Physical Review B **79**, 024408 (2009).

[12] C. R. Laumann, S. A. Parameswaran, S. L. Sondhi, and F. Zamponi, Phys. Rev. B **81**, 174204 (2010).

[13] D. P. Arovas and A. Auerbach, Phys. Rev. B **38**, 316 (1988).

[14] N. Read and S. Sachdev, Phys. Rev. Lett. **62**, 1694 (1989).

[15] I. Affleck, D. P. Arovas, J. B. Marston, and D. A. Rabson, Nuclear Physics B **366**, 467 (1991).

[16] M. Greiter and S. Rachel, Physical Review B (Condensed Matter and Materials Physics) **75**, 184441 (2007).

[17] S.-Q. Shen, Phys. Rev. B **64**, 132411 (2001).

[18] Z. Nussinov and G. Ortiz, Annals of Physics **324**, 977 (2009).

[19] S. Chen, C. Wu, S.-C. Zhang, and Y. Wang, Phys. Rev. B **72**, 214428 (2005).

[20] S. Östlund and S. Rommer, Phys. Rev. Lett. **75**, 3537 (1995).

[21] G. Vidal, Phys. Rev. Lett. **93**, 040502 (2004).

[22] F. Verstraete and J. I. Cirac, Phys. Rev. A **70**, 060302 (2004).

[23] D. Perez-Garcia, F. Verstraete, M. M. Wolf, and J. I. Cirac, eprint arXiv:quant-ph/0608197 (2006).

[24] Z. Y. Xie, J. Chen, J. F. Yu, X. Kong, B. Normand, and T. Xiang, ArXiv e-prints (2013).

[25] N. Read and S. Sachdev, Phys. Rev. Lett. **66**, 1773 (1991).

[26] P. Corboz, K. Penc, F. Mila, and A. M. Läuchli, Phys. Rev. B **86**, 041106 (2012).

[27] L. Muechler, J. Maciejko, T. Neupert, and R. Car, ArXiv e-prints (2014).

[28] S. A. Parameswaran, I. Kimchi, A. M. Turner, D. M. Stamper-Kurn, and A. Vishwanath, Phys. Rev. Lett. **110**, 125301 (2013).

[29] I. Kimchi, S. A. Parameswaran, A. M. Turner, F. Wang, and A. Vishwanath, Proceedings of the National Academy of Sciences **110**, 16378 (2013).

[30] S. A. Parameswaran, A. M. Turner, D. P. Arovas, and A. Vishwanath, Nature Physics **9**, 299 (2013).

[31] K. Chen, A. M. Ferrenberg, and D. Landau, Journal of applied physics **73**, 5488 (1993).

[32] R. Moessner and J. T. Chalker, Phys. Rev. B **58**, 12049 (1998).

[33] J. T. Chalker, P. C. W. Holdsworth, and E. F. Shender, Phys. Rev. Lett. **68**, 855 (1992).

[34] O. I. Motrunich and A. Vishwanath, Phys. Rev. B **70**, 075104 (2004).

[35] C. Wu, J.-p. Hu, and S.-c. Zhang, Phys. Rev. Lett. **91**, 186402 (2003).

[36] A. V. Gorshkov, M. Hermele, V. Gurarie, C. Xu, P. S. Julienne, J. Ye, P. Zoller, E. Demler, M. D. Lukin, and A. M. Rey, Nat Phys **6**, 289 (2010).

[37] D. S. Fisher and M. P. Fisher, Physical review letters **61**, 1847 (1988).

[38] S. Gazit, D. Podolsky, A. Auerbach, and D. P. Arovas, Physical Review B **88**, 235108 (2013).

[39] M. P. Fisher, P. B. Weichman, G. Grinstein, and D. S. Fisher, Physical Review B **40**, 546 (1989).

[40] S. Chakravarty, B. I. Halperin, and D. R. Nelson, Physical Review B **39**, 2344 (1989).

[41] T. Vojta, J. Crewse, M. Puschmann, D. Arovas, and Y. Kiselev, Physical Review B **94**, 134501 (2016).

[42] N. Read and S. Sachdev, Physical review letters **66**, 1773 (1991).

[43] O. Tchernyshyov and S. Sondhi, Nuclear Physics B **639**, 429 (2002).

[44] D. P. Arovas and A. Auerbach, Physical Review B **38**, 316 (1988).

[45] P. Titum, E. Berg, M. S. Rudner, G. Refael, and N. H. Lindner, Physical Review X **6**, 021013 (2016).

[46] S. Sachdev and K. Park, Annals of Physics **298**, 58 (2002).